Ocean Engineering 314 (2024) 119657

Contents lists available at ScienceDirect

Ocean Engineering

journal homepage: www.elsevier.com/locate/oceaneng

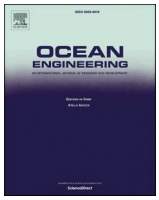

Research paper

The reliability of pre-deformation to control lateral buckling of pipelines: An evaluation based on observed embedment trends

Jayden Chee [a,*], Phil Watson [a], David White [a,b], Alastair Walker [a]

[a] University of Western Australia (UWA), Perth, Australia
[b] University of Southampton, UK

ARTICLE INFO

Keywords:
Subsea pipeline
Pipeline lateral buckling
Pre-deformed pipeline (PDP)
High pressure
High temperature (HPHT)
Pipeline
Soil interaction (PSI)
Out-of-Straightness (OOS)

ABSTRACT

Pre-deformation of a pipeline into a continuous sinusoidal wave-like form has been shown to be effective at controlling lateral buckling of subsea pipelines due to a substantially lower axial stiffness and the limiting of maximum strain at any location. This paper explores the feasibility and reliability of using such an approach, with an existing operating pipeline, which was installed using zero-radius bend (ZRB) initiator structures, used for comparison. Survey data of the pipeline profile and seabed bathymetry are adopted along with the pipe-soil interaction (PSI) inputs from the original design allowing a like-for-like comparison of the two approaches to management of lateral buckling. The comparison shows that, for the assumptions made in the numerical modelling, use of a pre-deformed pipeline results in lower strain than using ZRBs. Furthermore, the performance of the pre-deformed pipeline is robust, and shown to be unaffected by uncertainties in horizontal out-of-straightness, PSI input and seabed features. This study shows that pre-deformed pipelines can be an effective alternative for controlling the lateral buckling of subsea pipelines, which eliminates the need for buckle initiation structures to be installed along the pipeline route. This provides impetus for further work on installation methodologies to create the required level of pre-deformation.

1. Introduction

Subsea pipelines subjected to high temperature and high pressure (HTHP) can buckle laterally or vertically (upheaval) due to the build-up of compressive force associated with restraint from friction between the pipeline and seabed. If buckling is not properly controlled, severe structural failure may occur. Recommended practice DNV RP F110 (Det Norske Veritas, 2021) aims to accommodate thermal expansion by encouraging the pipeline to buckle at discrete locations along its length, at positions separated by the 'virtual anchor spacing' or VAS. If the VAS is small, there is less axial feed-in to the buckle, which reduces the lateral deflection and strain in the buckle. Fig. 1 illustrates the concept of VAS for a buckled pipe.

Zero-Radius Bend (ZRB) buckle initiators have been a preferred method for controlling lateral buckling for many subsea pipelines around the world, including offshore Australia, as they provide high reliability for controlling the VAS length – thereby creating certainty in the thermal expansion that feeds into individual buckles at designated (planned) locations. This ensures that the strain observed at each buckle is not excessive, while preventing unplanned buckling at other locations (Peek and Kristiansen, 2009).

However, the use of ZRBs, or other forms of engineered out-of-straightness such as sleepers, creates spans on each side of the support, which on a mobile seabed may grow to levels that are unacceptable for fatigue due to scour (Mamoon et al., 2023). This is particularly evident on the North West Shelf of Australia, where existing literature has reported significant changes in embedment and span length of pipelines in regions subject to sediment mobility (Rodriguez et al., 2013; Hou et al., 2023).

An alternative approach to control lateral buckling is to utilize a pipeline that is continuously pre-deformed prior to installation, as reported by Chee et al. (2018, 2019). This method has the benefit of eliminating engineered buckle initiators, saving cost and installation risk. Pre-deformed pipelines (PDP) differ from the existing residual curvature method (RCM, Endal et al., 2014; Endal and Nystrom, 2015) as the pipeline is pre-deformed continuously throughout the length, rather than being pre-deformed at specific planned buckle positions along the pipeline. Chee et al. (2018, 2019) discuss the theory behind and behaviour of a PDP, and show that they can operate safely at elevated temperatures without the need for other (expensive) initiation

* Corresponding author.
E-mail address: jay.chee@research.uwa.edu.au (J. Chee).

https://doi.org/10.1016/j.oceaneng.2024.119657
Received 18 September 2024; Received in revised form 20 October 2024; Accepted 27 October 2024
Available online 4 November 2024

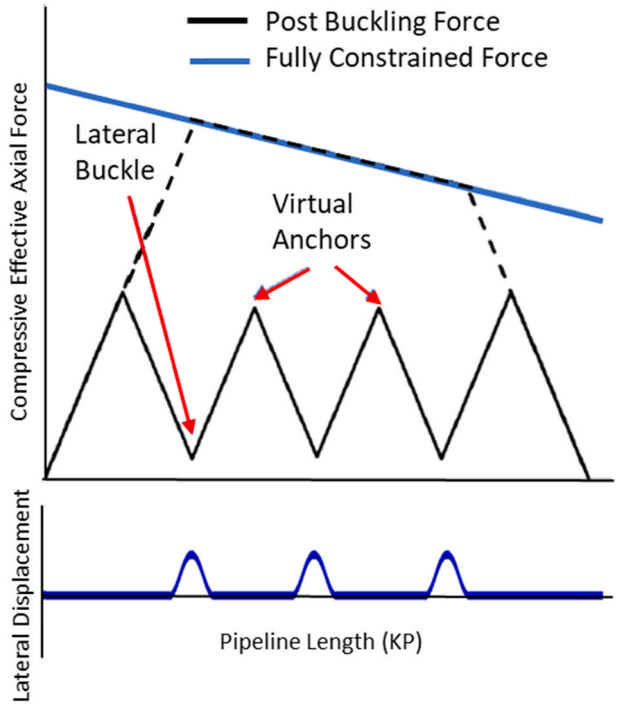

Fig. 1. Illustration of VAS formation along a buckled pipe (Det Norske Veritas, 2021).

methods. The performance of a PDP is shown to be robust and not affected by two of the key uncertain design variabilities: those being the as-laid horizontal out-of-straightness (HOOS) and the lateral pipe-soil interaction (PSI). This finding is due to the self-governing behaviour of PDPs, whereby they redistribute axial expansion locally and continuously through lateral movement along the entire pipeline, therefore minimizing the concentration of strain that occurs at isolated buckles, separated by the VAS.

The present study applies the method of continuous PDP as a counterfactual comparison with an existing pipeline on the North West Shelf, which was installed using Zero Radius Bend (ZRB) structures. This comparison explores the 'what if' scenario of using a PDP solution instead of ZRBs, taking advantage of the realism of the case study pipeline, which is supported by as-laid survey data and extensive PSI design work. The aim is to assess whether PDP could be used as an alternate and effective approach to control lateral buckling in scenarios similar to the case study.

We recognise that extensive work was undertaken to design the case study pipeline for thermal expansion and lateral buckling, and the present study is not intended to replicate the full design process. Where necessary, simplified assumptions have been made to produce a comparison with the ZRB case. Regardless, it has been possible to meet the overall objective by comparing the ZRB and PDP approaches using the same pipe parameters, seabed bathymetry, in-operation embedment condition, functional loads and pipe-soil interaction inputs.

To illustrate a typical PDP design, after installation on a natural undulating seabed, Fig. 2(a) illustrates the PDP geometry (top view) with a prescribe wavelength, L_ω and amplitude, ω_o, in the lateral direction, while Fig. 2 (b) shows an isometric view of the pre-deformed pipeline on an undulating seabed from the case study. In the previous work (Chee et al., 2018, 2019) the pipeline pre-deformation geometry of 0.7m amplitude every 4 joints (or 48m wavelength) was studied.

Installation of a PDP is not the subject of this paper. The practical feasibility of PDP manufacture and installation has been studied by previous published work such as Vermeulen (1995) and PDPs have been successfully installed in the past for controlling upheaval buckling (Lanan and Barry, 1992). To routinely install typical pipelines as PDPs requires specialised equipment on the lay vessels, which is not available in the current offshore market. This study aims to strengthen the motivation and business case for developing PDP installation technology.

The first part of this paper presents different configurations of pre-deformation, which were studied in order to select the optimal configuration to be used when modelling the installed pipeline. The second part of the paper compares the behaviour of the PDP with both a straight pipeline and with the same pipeline installed using zero radius bend (ZRB) structures (matching the reality of the case study pipeline). Each model was analysed using two different PSI scenarios, first using constant PSI parameters along the pipeline and the second using variable inputs, dependent on the observed embedment. The PSI inputs were adopted from the analysis used in the original case study design, and adapted for the second PSI case by taking into account the actual (surveyed) pipeline embedment, which was made available to the authors.

2. Design parameters

Table 1 summarises the pipeline and operating conditions adopted to study the characteristic properties of a PDP subjected to high operating temperature and pressure. No external pressure is applied in the modelling as this has minimal effect on lateral buckling – with the build-up of effective axial force being due to changes in internal pressure and temperature relative to the as-laid condition. The pipeline length selected for this study is 4.8 km, which is only a partial length of the actual pipeline and was selected based on multiples of a 12m pipe joint, i.e. 400 pipe joints.

The material stress-strain curve was generated using the Ramberg-Osgood relationship and the parameters in Table 1 (material yield strength, tensile strength and Young's Modulus of Elasticity) and is presented in Fig. 3. All relevant parameters are assumed to be invariant with temperature.

3. Pre-deformed Pipeline Axial stiffness (analytical)

An analytical expression for the axial stiffness of a pre-deformed pipeline as a function of deformation wavelength and amplitude is shown in Fig. 4. The axial stiffness ratio, K_p/K_s, is the stiffness of the pre-deformed pipeline relative to the straight pipeline. The axial stiffness of the pre-deformed pipeline, K_p, uses a simplified linear elastic formulation and is based on equations derived and published in Chee et al. (2018) (Eqn. (1)). Despite this being an elastic analysis, K_p varies with the pipeline axial force due to geometric non-linearity.

$$K_p = \frac{1}{\frac{L_T}{EA_s} - \frac{\pi^2\omega_o^2}{2L_w P_{cr}\left(\frac{P_{ax}}{P_{cr}}-1\right)^3}} \tag{1}$$

where.

L_T = length of pipe
L_ω = wavelength of the sinusoidal curve
ω_o = maximum lateral amplitude of the sinusoidal curve (at $L_\omega/2$)
E = Young's Modulus of Elasticity
A_s = cross-sectional area of the pipe
P_{ax} = axial force along the pipeline
P_{cr} = critical buckling force

$$= \frac{4\pi^2 \mathrm{EI}}{{L_w}^2}$$

I = Second Moment of Pipe Area
K_s is the stiffness of a straight pipeline given by EA/L_T.

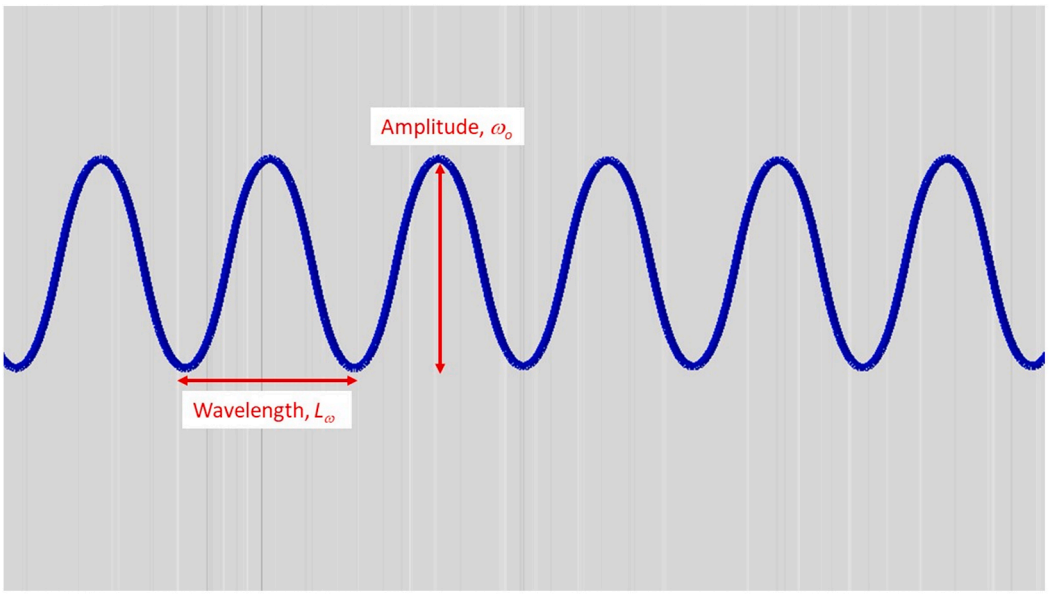

(a) Pre-deformed Pipeline Geometry

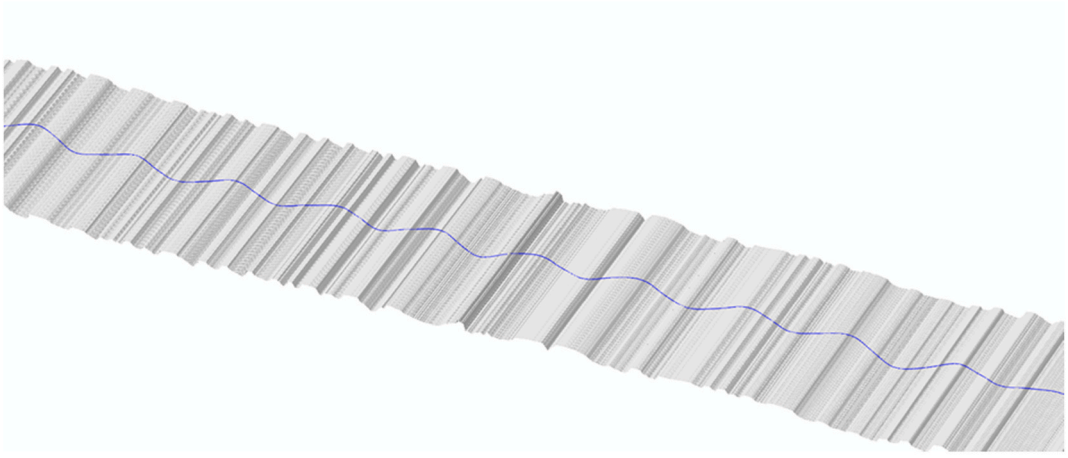

(b) Pre-deformed pipeline on an undulating seabed

Fig. 2. Illustration of a laterally pre-deformed pipeline.

As can be seen in Fig. 4, the longer the wavelength and the larger the amplitude, the lower the axial stiffness. The benefits of low axial stiffness were demonstrated in Chee et al. (2018), who highlighted that this makes it harder for the pipeline to buckle, i.e higher temperature and pressure is needed to build up the required effective axial force to initiate buckling.

The pipeline with a pre-deformation wavelength of $L_\omega =$ 96m has a significantly lower stiffness ratio than the straight pipe, as shown in Fig. 5. The calculations show that a pre-deformed pipeline with 96m wavelength and amplitude of $\omega_0 = 0.6$m has 0.4% of the stiffness of a straight pipeline (at zero axial force), which decreases further to 0.1% for $\omega_0 = 12$m.

4. Methodology adopted to match as-surveyed pipeline vertical profile for numerical modelling

The as-surveyed post-hydrotest embedment data was used in this study to provide a realistic distribution of pipe-seabed interaction behaviour along the pipeline route. The following section outlines the methodology used to replicate the measured pipeline embedment in the numerical model, and determine the appropriate PSI resistance forces for the numerical modelling.

The post-hydrotest seabed bathymetry and the vertical profile of the invert of the case study 16-inch pipeline is shown in Fig. 6, based on survey data that was available every 2 m along the pipeline.

Fig. 7 provides a statistical assessment of the post-hydrotest embedment (water-filled) as extracted from the field survey water depth and pipeline vertical profile shown in Fig. 6. In Fig. 7, the embedment is defined z/D, where z refers to the buried depth from the seabed surface to the bottom of the pipeline and D refers to the pipeline diameter including external coating.

In the post-hydrotest survey, 48% of the total pipeline was found to be embedded. The post-hydrotest embedment ranges from zero (at the edge of spans), to a maximum of 1.1 times the pipe outer diameter, with

Table 1
Pipeline parameters.

Parameters	Unit	Value
Pipe Outer Diameter, *OD*	m	0.4064 (16in)
Pipe Wall Thickness, *WT*	mm	23.6
Pipe External Coating, t_{ext}	mm	32.44
Pipe Submerged Weight, $W_{s,empty}$ (Empty)	N/m	786
Pipe Submerged Weight, $W_{s,water}$ (Hydrotest/Water-Filled)	N/m	1805
Pipe Submerged Weight, $W_{s,op}$ (Operating)	N/m	905
Pipeline Total Length, L_T	km	4.8
Hydrotest Temperature, T_{hyd}	°C	17.5
Maximum Operating Temperature, T_{op}	°C	140
Ambient Temperature, T_{amb}	°C	9.4
Hydrotest Pressure, P_{hyd}	bar	38.6
Maximum Operating Pressure, P_{op}	bar	170
Pipeline Material Young's Modulus, *E*	GPa	205
Coefficient of Thermal Expansion, α	1/°C	1.18×10^{-5}
Residual Lay Tension, T_{Res}	kN	350
Specified Minimum Yield Strength, *SMYS*	MPa	440
Specified Minimum Tensile Strength, *SMTS*	MPa	545
Poisson's Ratio, ν	–	0.3

almost 74% of the embedded length being deeper than 0.5*D*. The most common embedment is in the range 0.6–0.7*D*.

The embedment profile of the pipeline in the numerical modelling was aligned with the post-hydrotest as-survey profile by creating (in the numerical model) a seabed that is truncated by taking the minimum of the vertical profiles for the seabed and the pipeline (Fig. 8 – for clarity, only Kilometer Point (KP) 1.5–2.0 km along the pipeline is shown). This avoids the need to define a vertical spring appropriate for pipelay, while ensuring the numerical model captures the pipeline vertical out-of-straightness (spans and embedment) accurately.

Using the 'truncated' seabed, a straight pipeline could then be modelled that matches the as-surveyed post-hydrotest pipeline profile. The number and length of spans were assessed based on the survey data and compared to the post-hydrotest survey pipeline as shown in Fig. 9 (a). It is clear that the as-surveyed post-hydrotest vertical profile of the pipeline matches the adopted profile except at the ZRB locations – which is to be expected because the numerical model excludes these. These span lengths were omitted manually in the analysed seabed bathymetry. The profile is expanded between the KP 1.5 to 2.0 along the pipeline in Fig. 9(b), showing the comparison of the pipeline profile modelled by FEA and the survey pipeline.

Fig. 10 shows the percentages of the pipeline that are spanning and are on the seabed for both the FEA model and actual survey data (post-hydrotest). The FEA model and survey data both show around 52% of the 4.8 km pipeline length is in span.

To further illustrate the closeness of the FEA model and survey data, the confusion matrix in Fig. 11 indicates 49% true positive (where both FEA and survey are in span) and 44.6% true negative (where both FEA and survey pipeline shows no span). This leaves only 6.3% false cases in the FEA model, of which 3.3% are false positive (where FEA predicts a span but this is not evident in the survey). Given the low percentage of false cases, the 'truncated' seabed approach is shown to be adequate to mimic the real case study pipeline, and then compare with a PDP on the same realistic seabed. Accordingly, the embedment profile from the FEA analysis can be used to select the PSI parameters, which is detailed in the next section.

5. Methodology to select PSI inputs for numerical modelling

Fig. 12 presents a flowchart describing the methodology used to select PSI inputs for numerical modelling, using the as designed and available survey embedment data. The PSI parameters generated during the original design phase of this pipeline were made available for this study, and both the post-lay and post-hydrotest embedment data was provided. The approach was used to align design inputs and actual embedment data is outlined in the following sections.

5.1. As-designed pipe-soil interaction (PSI) data

Table 2 below presents the best estimate (BE) as-design pipe-soil interaction (PSI) inputs for as-laid, hydrotest and operating condition.

(1)Calculated based on total outer pipeline diameter, *D* of 0.471m (including external coating).

Fig. 13(a) presents the relationship between as-designed best estimate (BE) embedment and mobilisation distances for as-laid, hydrotest and operating condition, while Fig. 13(b) reports the associated friction factors – as taken from Table 2. Trendlines are fitted to each data set, with these relationships used to generate PSI inputs for embedment

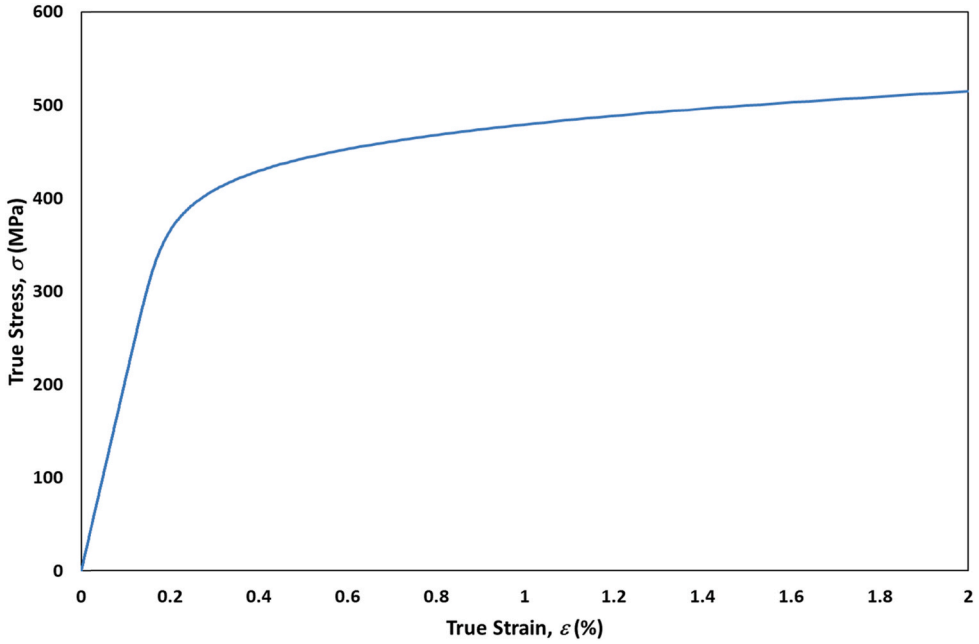

Fig. 3. Adopted true stress-strain curve for the pipeline carbon steel material.

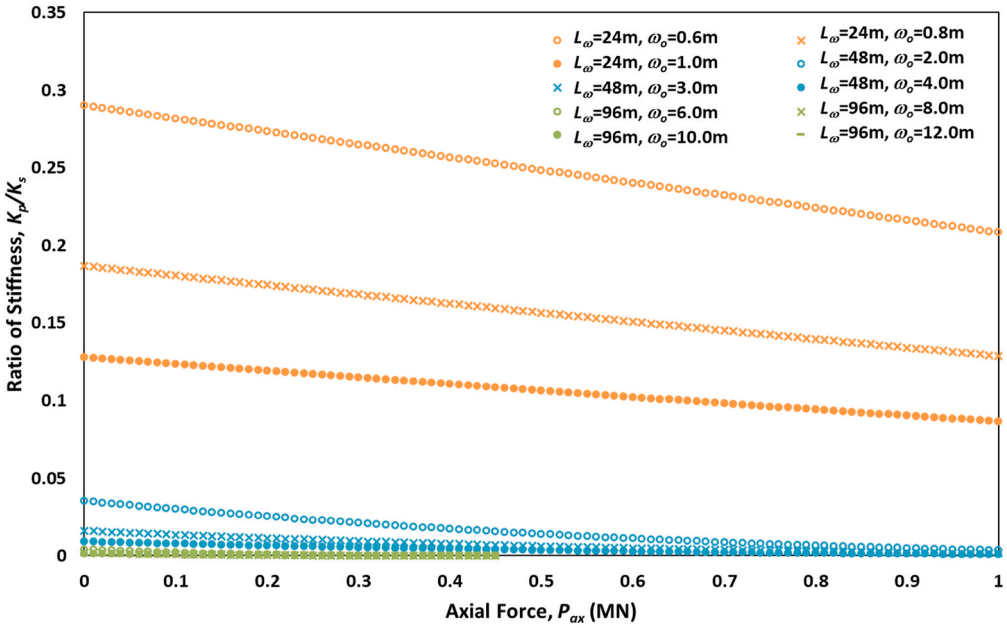

Fig. 4. Axial stiffness ratio of the pre-deformed pipeline.

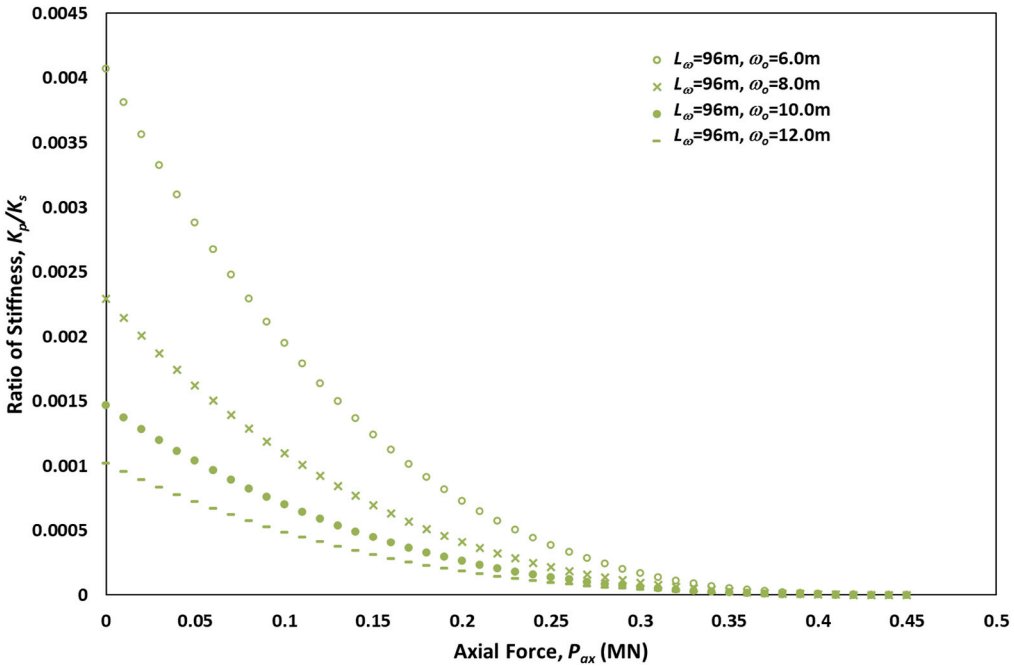

Fig. 5. Axial Stiffness Ratio of Pre-deformed Pipeline with 96m wavelength.

varying with KP along the pipeline, based on the numerical analysis using the post-hydrotest and operating condition surveys. In Fig. 13(b), lateral breakout friction is fixed at 0.68 (which is the lateral residual friction) for embedment of $z < 0.035$.

5.2. Survey embedment and pipe-soil interaction (PSI)

PSI inputs were derived from the as-surveyed seabed profile and the FEA bottom of pipeline profile, which combine to give pipeline embedment. Fig. 14 shows the resultant embedment, with positive values representing embedment and negative values indicating the pipeline is in span.

Removing the spans (for which no PSI input is required), the model embedment representing the post-hydrotest condition is shown in Fig. 15. Since the analysis is intended to reflect operating conditions (when the pipeline is lighter compared to the post-hydrotest conditions), but no survey data exists for this case, it was decided to increase the embedment by the difference between the calculated BE embedment in the as-designed post-hydrotest and operating conditions, which resulted in an increase in embedment by $\Delta z = 0.085$m ($\Delta z/D = 0.18$), and is attributed in the design analysis to seabed settlement and sediment movement (also shown in Fig. 15).

In order to investigate the effect of localised PSI input on the behaviour of the pre-deformed pipeline, FEA was undertaken using inputs at different spacing along the pipeline. This is illustrated in Fig. 16 for the post-hydrotest condition, which shows the survey embedment (at

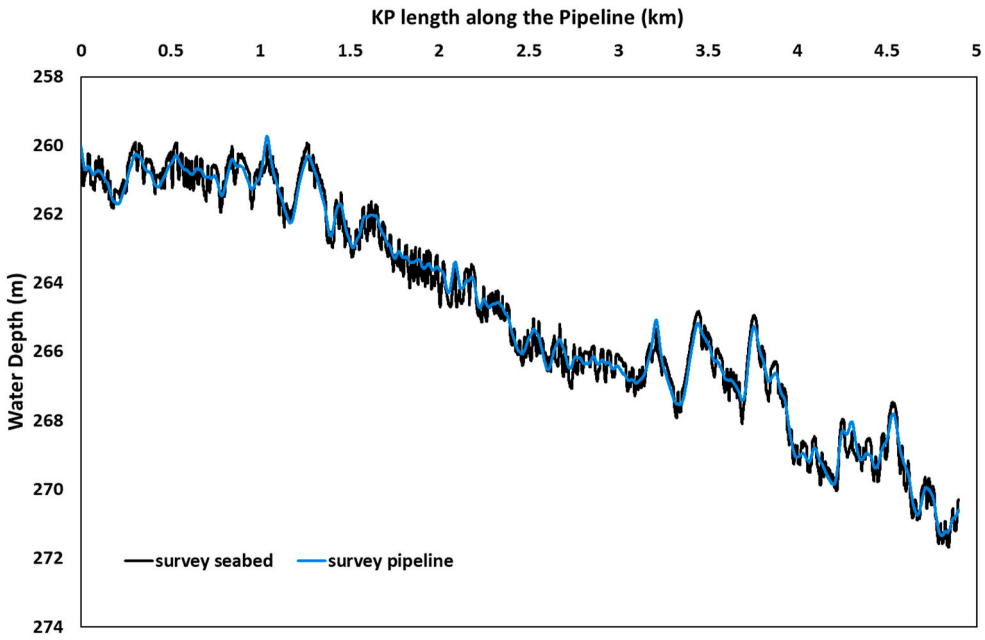

Fig. 6. As-survey post-hydrotest seabed and pipeline profile.

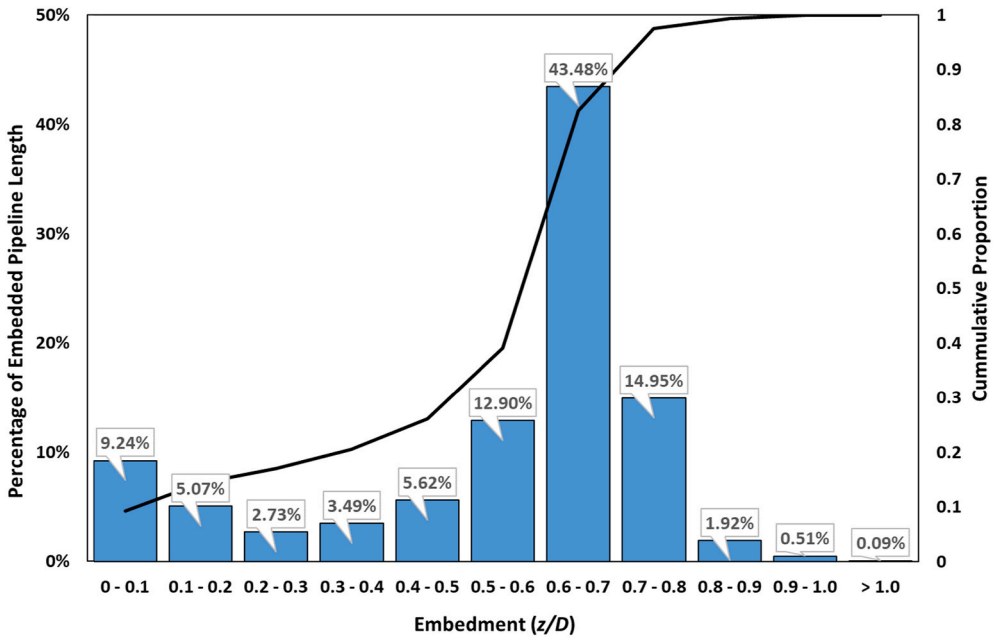

Fig. 7. Statistical data of the post-hydrotest survey embedment.

0.2m spacing along the pipeline) and the embedment (used to generate PSI input) for two different cases: the first with embedment averaged over 5m spacing, and the second for the case of a single uniform embedment (equal to the average surveyed value, $z = 0.261$m, $z/D = 0.55$. For clarity, the data is expanded between KP 1.5 to 2.0 in Fig. 16 (b).

Fig. 17 presents the adopted pipeline embedment for operating conditions. Similar to post-hydrotest, the average embedment over 5m spacing and a single (average) embedment, $z = 0.304$m ($z/D = 0.64$) for the operating condition are presented (with detail shown for KP 1.5–2.0 km in Fig. 17(b).

The resultant BE lateral mobilisation distances, BE axial friction factors, BE lateral breakout friction factors and BE residual friction factors for each post-hydrotest embedment at 5m is shown in Fig. 18. Note that the axial mobilisation distance is not shown as it is assumed constant (at 0.01m) for the entire pipeline. The (constant) average values for each of the mobilisation and friction factors is shown in these charts. Those for the operating condition are shown in Fig. 19.

In the operating condition, and as shown in Fig. 20, the influence of embedment on breakout resistance leads to breakout friction factors ranging from 0.68 (shallow embedment) to 8.9 (deep embedment), with a length-averaged breakout friction of 2.91. Slightly greater than 32% of the deeply embedded pipeline length has a breakout friction of 5.0 or more, while around 28% of the embedded pipeline is shallower which has breakout friction of 1.0 and less.

Using the above, an example of the axial and lateral friction responses are shown in Fig. 21(a) and (b) respectively for embedment between $0.1D$ and $1.0D$. For axial friction responses, embedment higher

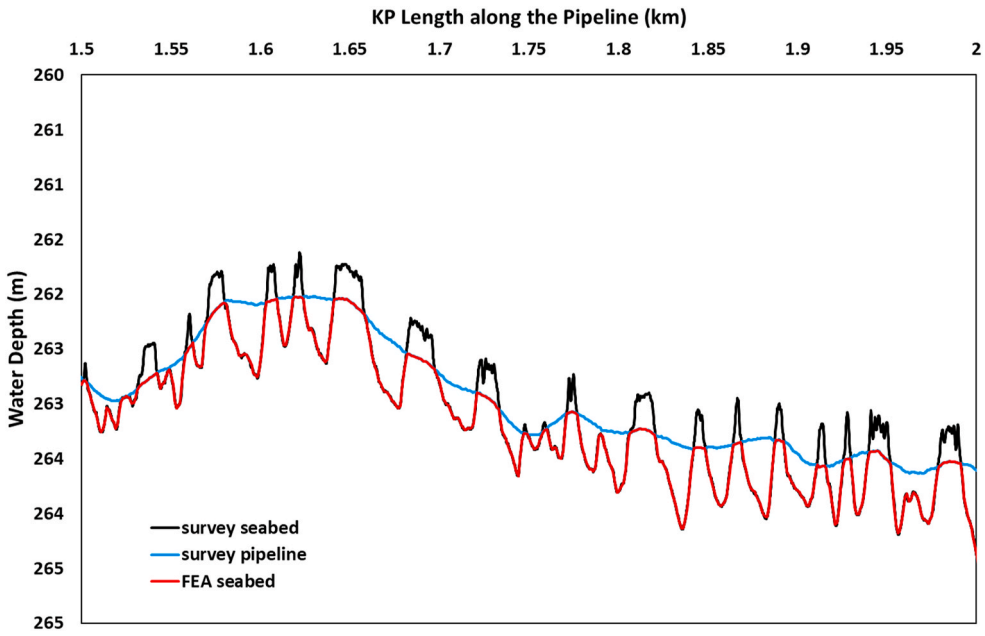

Fig. 8. 'Truncated' seabed in FEA

than 0.6*D* are not shown as they are similar with axial friction capped at 1.0.

6. Finite element analysis (FEA) modelling

6.1. Analysis cases

The finite element software ABAQUS (Abaqus Analysis User Manual, 2020) was used for all numerical simulations in this study. The following are the cases analysed to show the advantages of using a pre-deformed pipeline in controlling lateral buckling.

1. Case 1: Pre-deformed pipeline (PDP) on a realistic (and uneven) seabed.
2. Case 2: Pipeline with ZRB (as per the case study) on the same seabed.
3. Case 3: Straight pipeline without any buckling mitigation method on the same seabed.

6.2. Pipe elements

The pipe element used in ABAQUS is PIPE31H. This is a 3D two-node linear pipe element with 6 DOF at each node and numerical integration of material response at 32 integration points around the circumference.

6.3. PSI and seabed modelling

In all FEA calculations, the bathymetry and embedment is based on data from an existing pipeline, as explained previously, extrapolated horizontally in the lateral direction. Contact pairs were used to model the interaction between the pipeline and the seabed, while the ABAQUS user subroutine FRIC is used to capture the contribution from the independent axial and lateral components of the contact surface (noting this subroutine is necessary to account for a tri-linear lateral resistance). For simplicity, both axial and lateral resistance are assumed independent of the small vertical penetration of the slave surface, i.e. the pipe element penetration into the master surface, which implies a small increase in embedment, does not result in higher friction values.

6.4. Loading

The relevant submerged weight of the pipeline was simulated by applying a uniform distributed weight to the pipe element, with no external pressure applied. The initial temperature was taken to be 9.4 °C and operating temperature is 140 °C, with internal pressure of 170 bar. The operating temperature and pressure were applied simultaneously in constant increments.

6.5. Modelling steps for pre-deformed pipeline

For the pipeline section used as the basis of this paper, a 4.8 km-long straight pipe was initially positioned on a flat frictionless plane. One end of the pipeline was fixed in the axial and lateral directions while the other end was fixed in the lateral direction to prevent rigid body motion. The submerged weight of the empty pipeline was then applied. Rotation was then applied to each node about the vertical axis in order to plastically bend the pipeline into a sinusoidal shape in plan based on the prescribed wavelengths and amplitudes shown in the illustration in Fig. 2. The imposed rotations and displacements are then removed, and the pipeline partially springs back, and residual curvature and strain remains. This simplified method to initiate a pipeline numerical model has been used by other researchers analysing the residual curvature method and is adopted to avoid needing to model the complicated bending process, such as pipeline passing through a straightener in the reeling process (Bahrum et al., 2023; Cooper et al., 2017; Powell et al., 2019).

To simulate likely variability in the pre-deformation process, a random variation in each lobe's peak amplitude, up to ± 5% of the prescribed amplitude, ω_o, was included. The amplitude of successive lobes varies randomly within these ranges.

The assumed (random) out-of-straightness has a continuous uniform distribution given by the probability density function *f(x)* as shown in Eqn. (2).

$$f(x) = \begin{cases} \dfrac{1}{\beta - \alpha} & \text{for } \alpha < x < \beta \\ 0 \quad \text{for } x < \alpha \text{ and } x > \beta \end{cases} \tag{2}$$

where α and β are lower and upper bounds respectively.

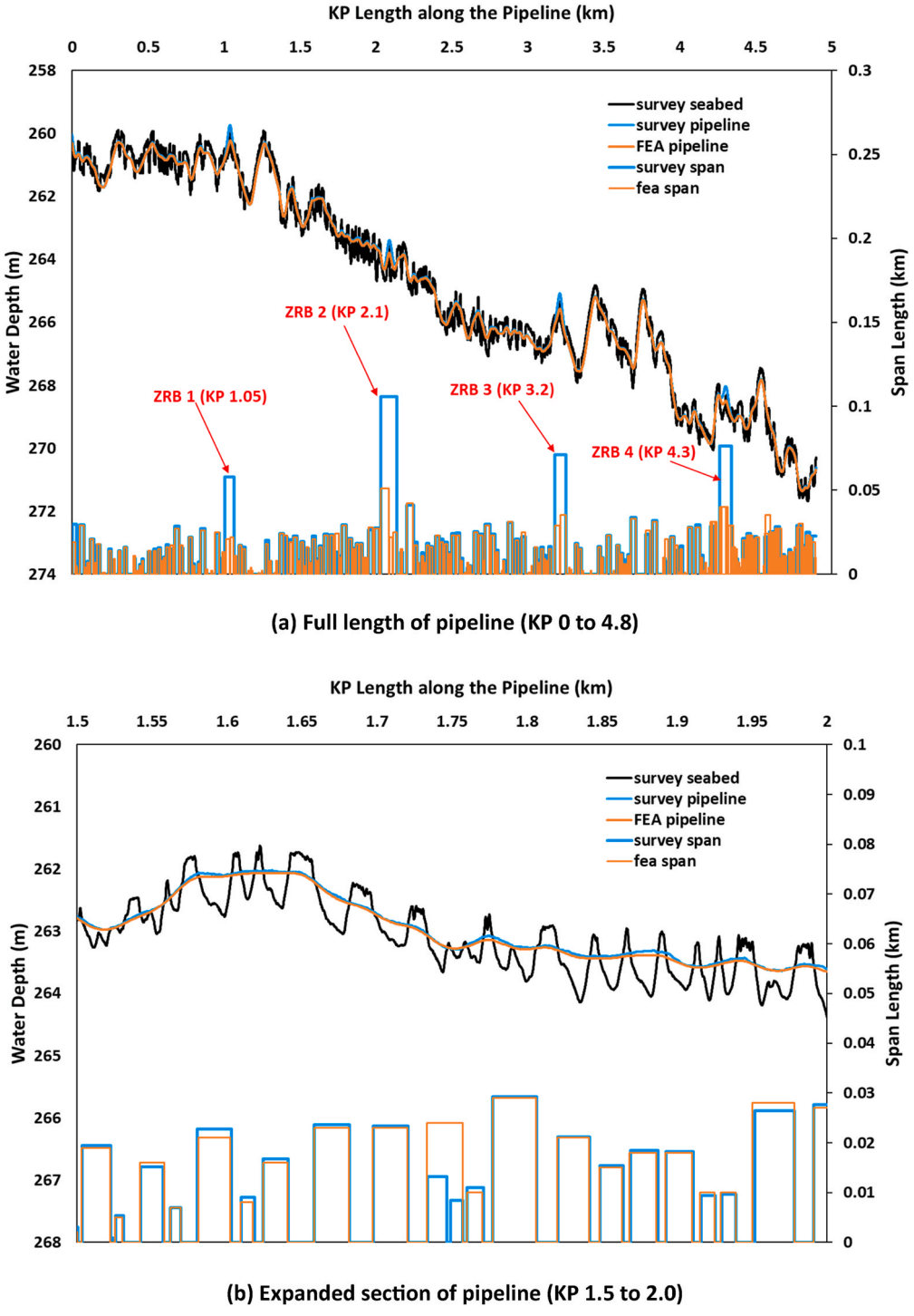

Fig. 9. Comparison between FEA pipeline profile and post-hydrotest survey pipeline.

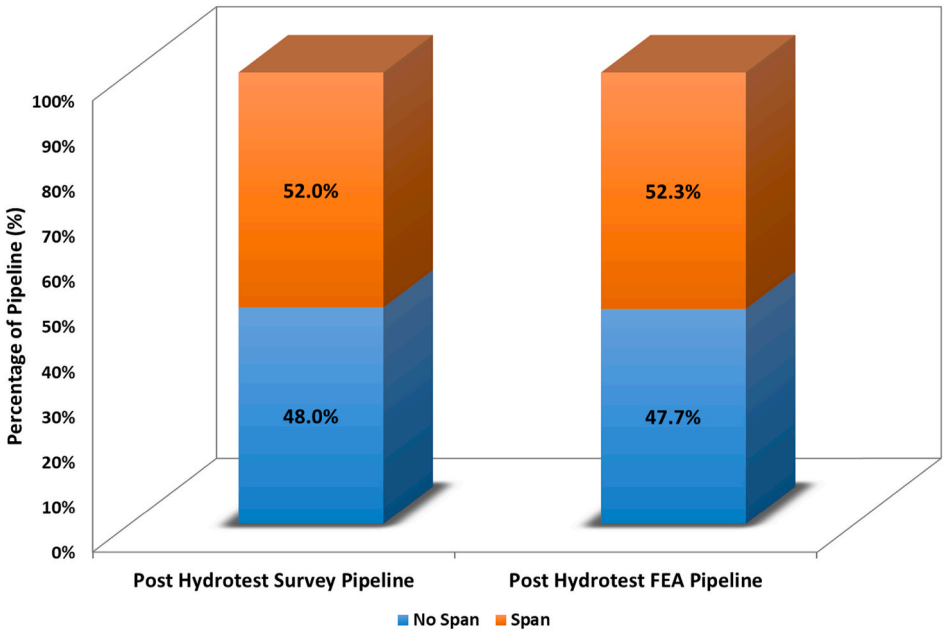

Fig. 10. Percentage of pipeline length with and without spans in post-hydrotest.

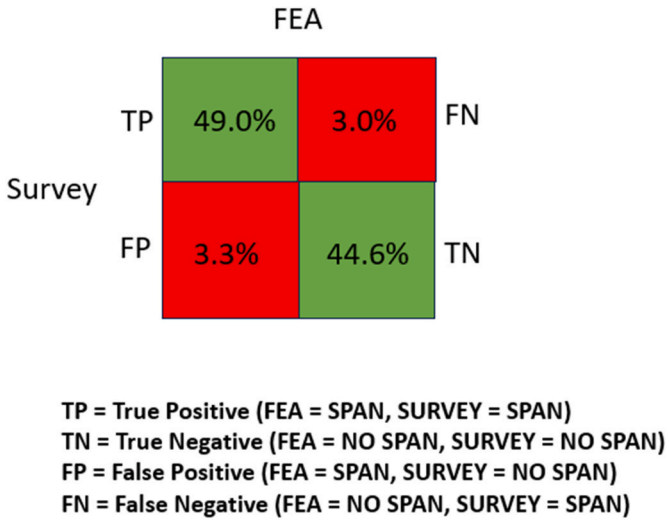

Fig. 11. Confusion matrix comparing the presence of spans in post-hydrotest survey and FEA.

A bottom lay tension of 350 kN (assumed for this analysis) was applied by pulling on the free end of the pipe, and the pipeline is lowered into the uneven seabed described in Section 4. The bottom tension is removed after introducing pipe-soil friction so that only residual tension remains in the pipeline. The pipeline ends are connected to spring elements with stiffness in both lateral and axial directions to mimic the spools at each end. All boundary conditions on the pipeline are released before the submerged weight, pressure and temperature of first the hydrotest and then the operating conditions are applied. The appropriate pipe-soil interaction and friction behaviours described in Section 5.2 corresponding to hydrotest and operating conditions was adopted.

6.6. Modelling steps for pipeline with ZRBs

The initial modelling procedure for the pipeline with ZRBs is the same as for the pre-deformed pipeline, except that it is not bent into sinusoidal lobes before being lowered onto the uneven seabed. Instead, the pipe is laid around ZRBs located at KP1.05, KP 2.1, KP 3.2 and KP4.3 (within this part of the pipeline). Each ZRB is modelled as a rigid circular beam with a vertical post, both with a diameter of 0.4m. Initially, the frictional contact is only activated between the start of the pipeline and the first buckle initiator, so that the remainder of the pipeline can move freely across the seabed. The friction coefficient between the pipeline and buckle initiator is assumed to be 0.3. The rest of the pipeline is left on a frictionless surface while the pipeline is rotated through a bend angle of 13° around the initiator vertical post to form the designed geometrical imperfection. Once this deflection is achieved, frictional contact is activated on the pipeline between the first for the second buckle initiator. This process is repeated until the pipeline is bent around all four ZRBs. Similar to the PDP, all boundary conditions on the pipeline are released before the PSI, submerged weight, pressure, temperature of hydrotest is applied, and then followed by the operating conditions.

7. Selection of PDP wavelength and amplitude

From the results presented in Fig. 4, it is clear that increasing the pre-deformation wavelength and amplitude produces a reduction in axial stiffness, which is effective in controlling lateral buckling. However, a trade-off exists when large amplitude pre-deformation is used – in that the pre-deformation itself can result in a high bending strain.

The analytical calculations presented in Fig. 4 do not take into account contact between the pipeline and seabed, i.e. PSI is not accounted for. Therefore, further analysis was undertaken using a 96m pre-deformation wavelength and constant values of average friction factor along the pipeline (shown as dashed lines in Figs. 18 and 19.

Fig. 22 below shows the maximum tensile strain versus the initial strain of the pre-deformed pipeline on the realistic uneven case study seabed for the pre-deformed pipeline with wavelengths of L_ω = 24m, 48m and 96m wavelength and different amplitudes, ω_0. The 24m wavelength has the highest maximum operating strain and is highly sensitive to the amplitude, as a small increase in amplitude results in a significant increase in strain. The maximum longitudinal strain for 48m wavelength is relatively constant for amplitudes of between 1 and 2m. However, a further increase in amplitude causes the strain to increase. The maximum longitudinal strain for the 96m wavelength is lowest across all 4 different amplitudes. The 10m amplitude has the lowest tensile strain at the operating condition (i.e. 140 °C and 170 bar) with

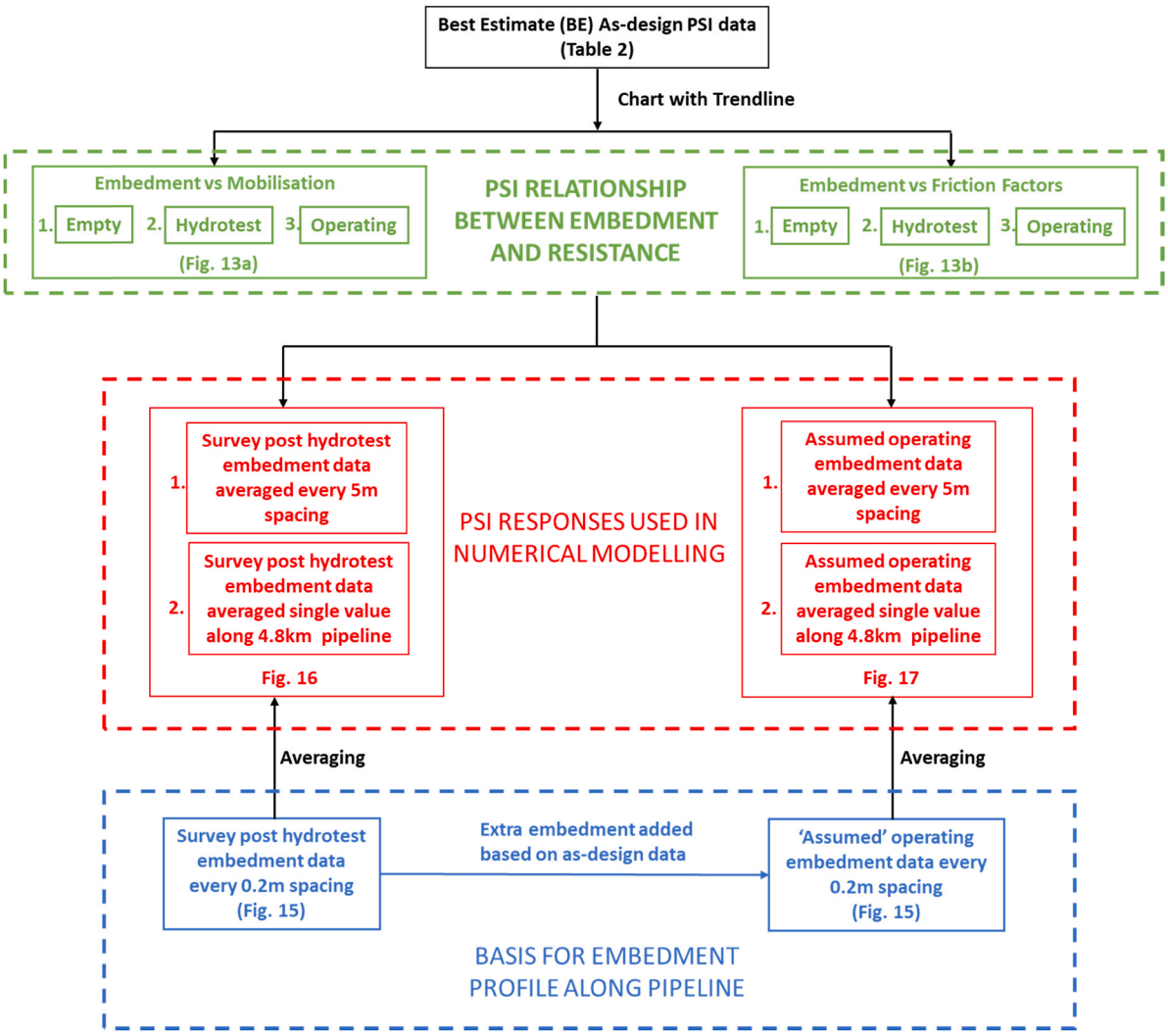

Fig. 12. Methodology flowchart for numerical modelling PSI inputs selection.

Table 2
Best estimate (BE) PSI data from original design report.

Parameters	Unit	As-Laid	Hydrotest	Operating
Pipeline Embedment, z/D	–	0.21	0.48	0.66
Pipeline Embedment, z[(1)]	m	0.099	0.226	0.311
Pipe-Soil Lateral Breakout Friction, $\mu_{L,BO}$	–	1.00	1.57	3.13
Lateral Breakout Mobilisation Distance, $d_{L,BO}$	m	0.21	0.06	0.08
Pipe-Soil Lateral Residual Friction, μ_L	–	0.70	0.64	0.70
Lateral Residual Mobilisation Distance, d_L	m	0.6	1.1	1.5
Pipe-Soil Axial Friction, μ_A	–	0.85	0.96	1.05
Axial Mobilisation Distance, d_A	m	0.01	0.01	0.01

(1) Calculated based on total outer pipeline diameter, D of 0.471m (including external coating).

the 6m and 12m cases resulting in a similar strain level. From this, it is concluded that the 96 m pre-deformation wavelength is robust – with low sensitivity to the achieved amplitude – and that the initial amplitude can vary ± 2m without significantly impacting the operating condition strain.

Fig. 23 presents the effective axial force variation for the pre-deformed pipeline as it transitions from ambient conditions of 9.4 °C to operating of 140 °C. Negative effective axial force indicates that the force is compressive while positive effective axial force indicates that the force is tensile. The 6m amplitude case buckles at a critical buckling temperate, T_{cr} of 33.5 °C, which increases to 47.1 °C for 8m amplitude and 52.7 °C for 10m amplitude. This critical buckling temperatures are taken at the buckle locations with the lowest initiation force (for each case). This suggests that the 6m amplitude case does not have sufficient pre-deformation to control lateral buckling in a stable manner, which is due to the existence of an unstable drop in effective axial force at 33.5 °C. In contrast, the pre-deformed pipeline with 10m amplitude exhibits no sudden decrease in effective axial force which makes it a stable buckle, representing a re-organizing of the sinusoidal lobes to accommodate the thermal expansion through steady increases in the lateral displacement. The 96m wavelength pre-deformed pipeline with 12m amplitude did not show an unstable buckle even at 140 °C. However, the final strain at the operating condition is higher than for the 10m amplitude case, reflecting the higher initial strain during bending of the pipeline.

Based on these findings, a 96m wavelength pre-deformation with 10m amplitude was considered optimum, and was selected as the adopted solution for the case study of the pipeline on the realistic observed seabed profile and embedment history.

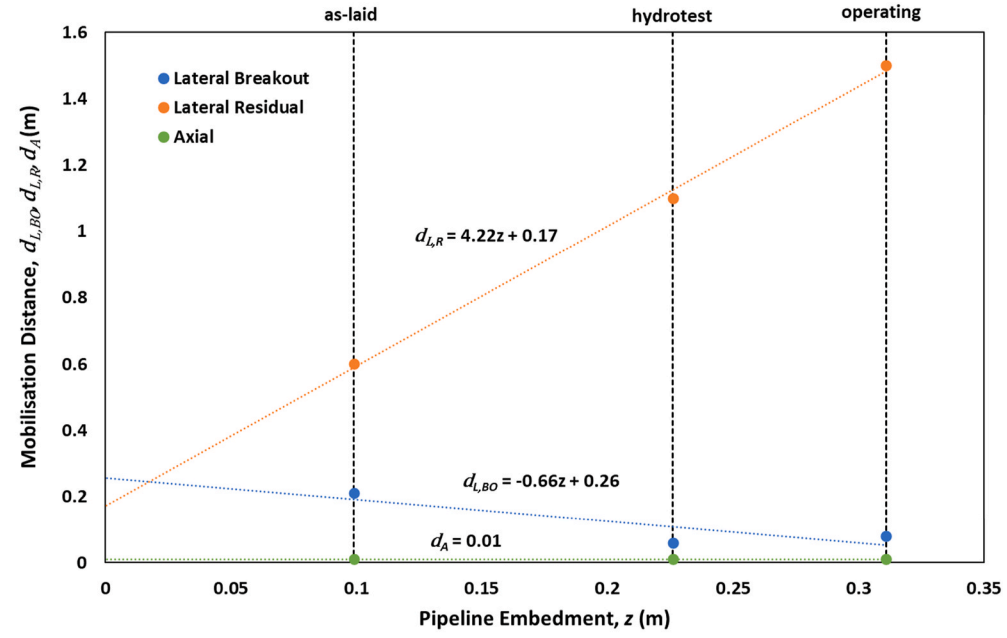

(a) Mobilisation Distance against Pipeline Embedment

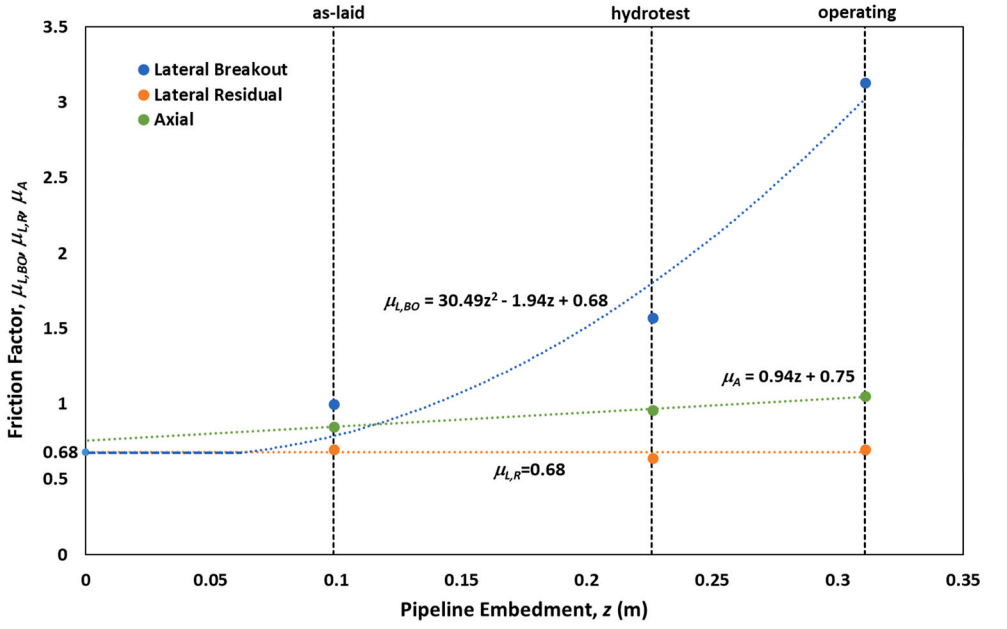

(b) Friction Factors against Pipeline Embedment

Fig. 13. As-design best estimate PSI.

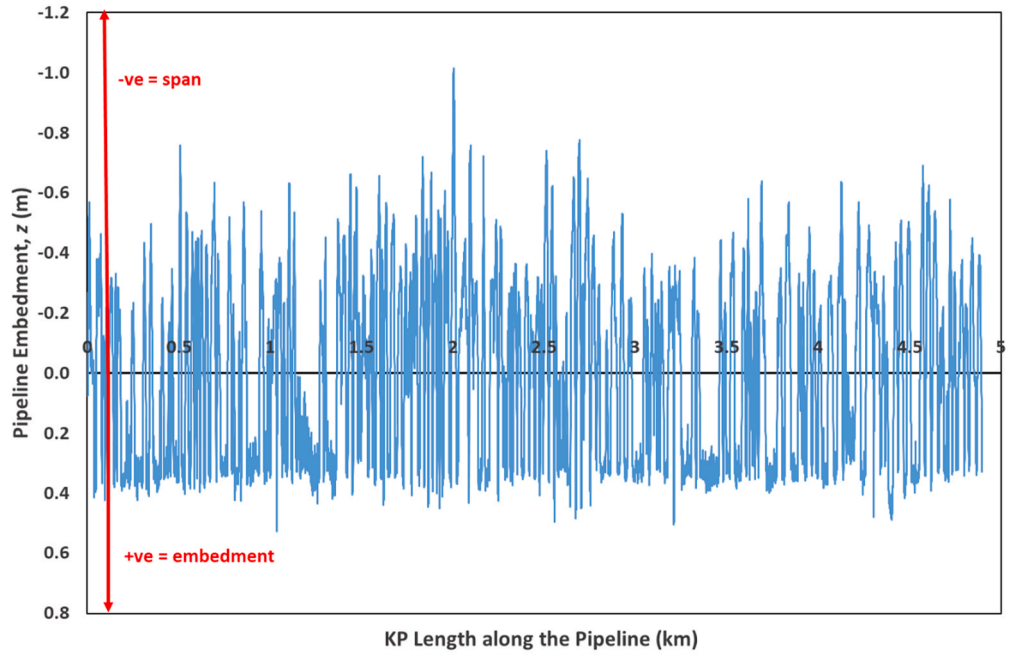

(a) Full length of pipeline (KP 0 to 4.8)

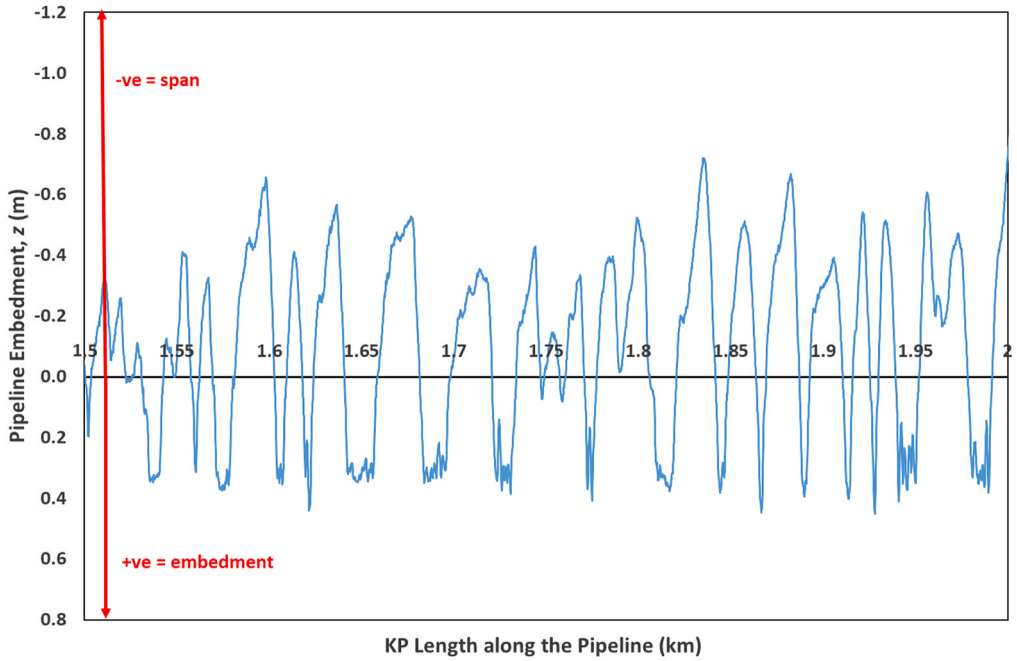

(b) Expanded section of pipeline (KP 1.5 to 2.0)

Fig. 14. Pipeline span and embedment along the seabed during post-hydrotest.

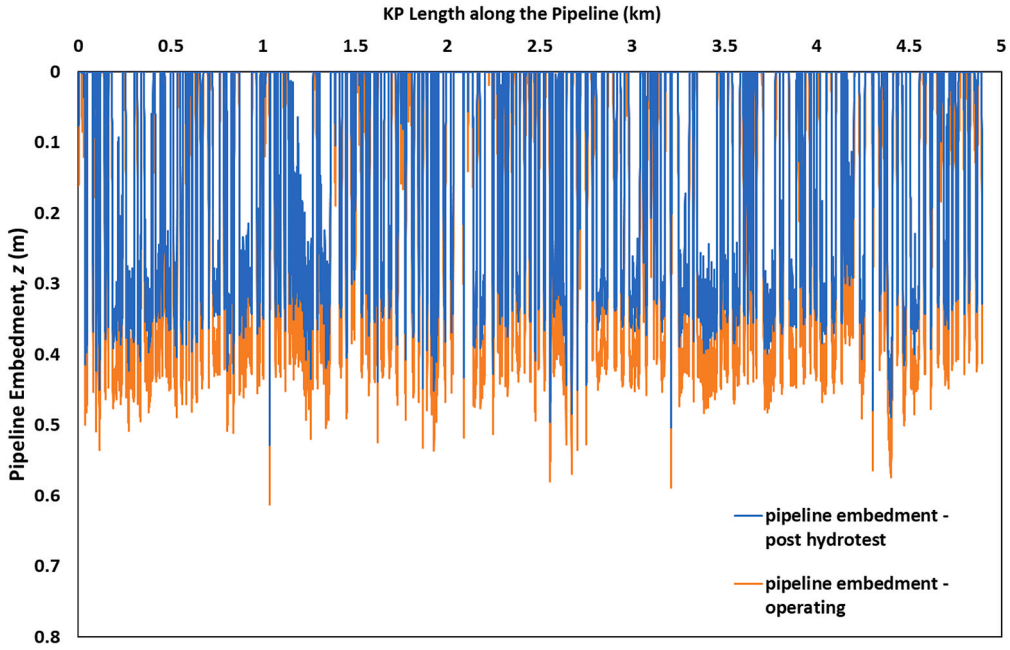

(a) Full length of pipeline (KP 0 to 4.8)

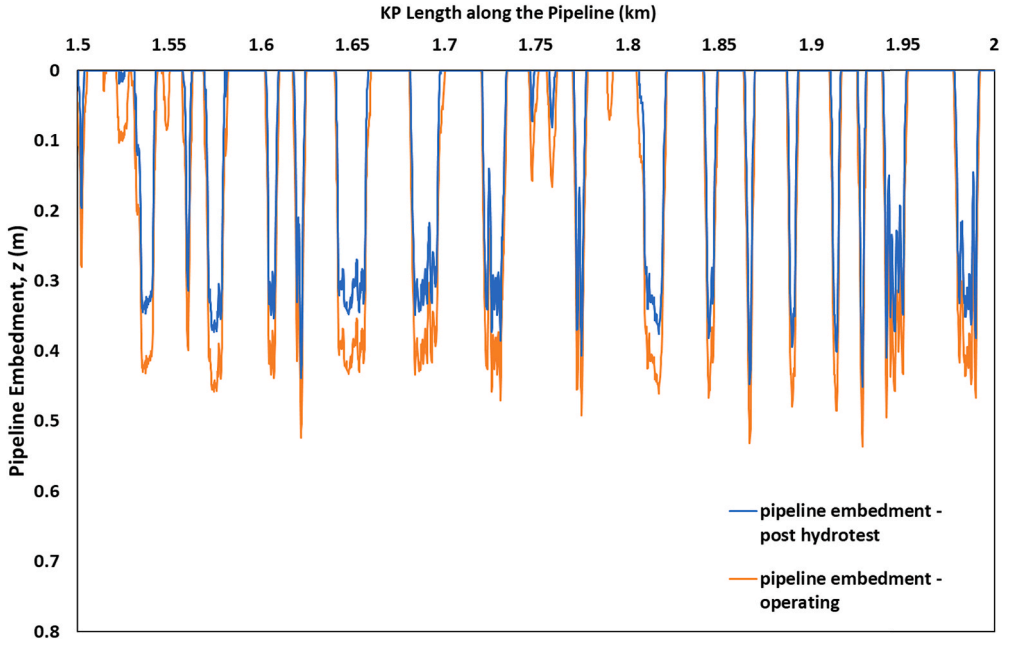

(b) Expanded section of pipeline (KP 1.5 to 2.0)

Fig. 15. Adopted pipeline embedment in the post-hydrotest and operating condition.

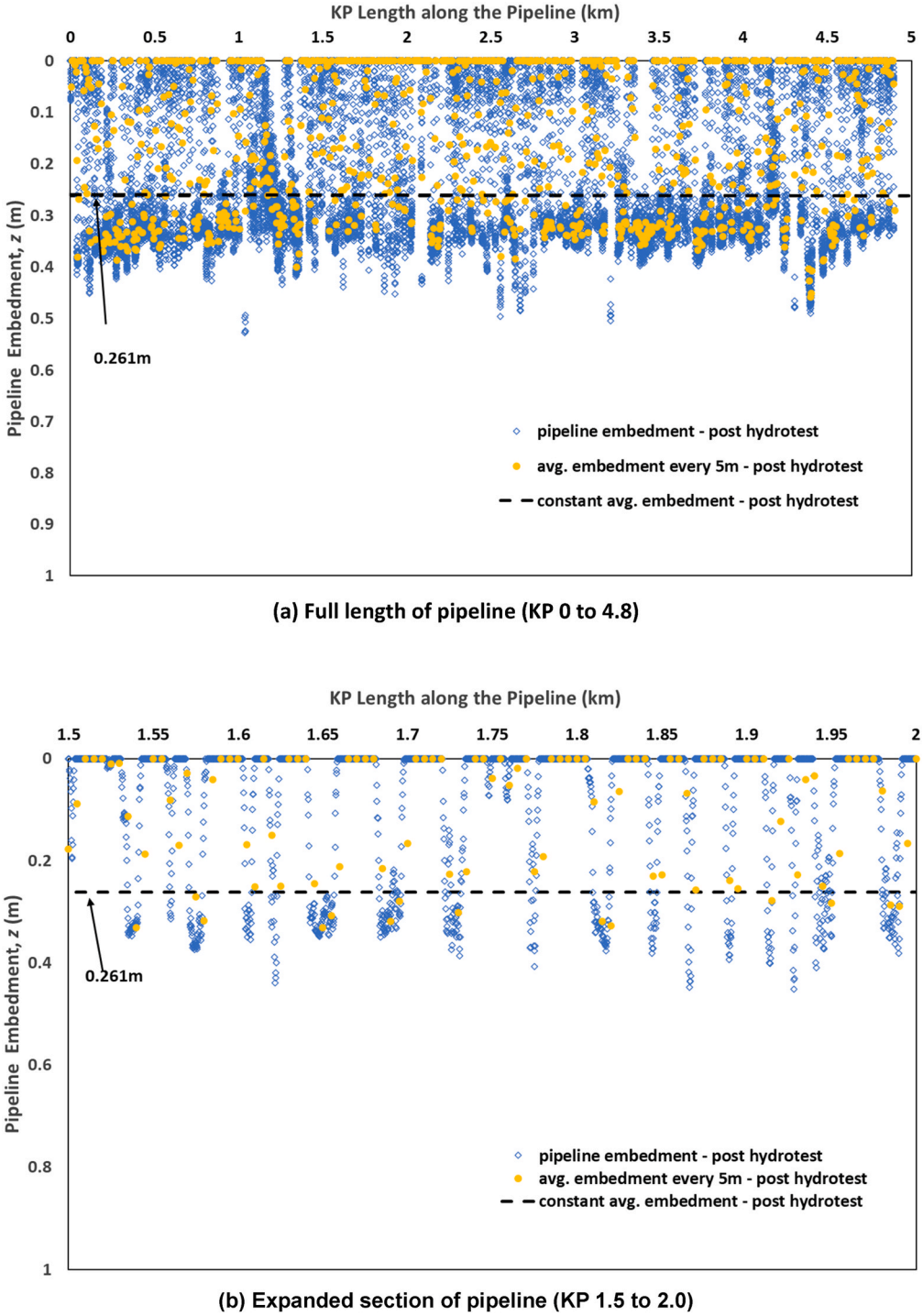

Fig. 16. Pipeline post hydrotest condition average embedment along the seabed.

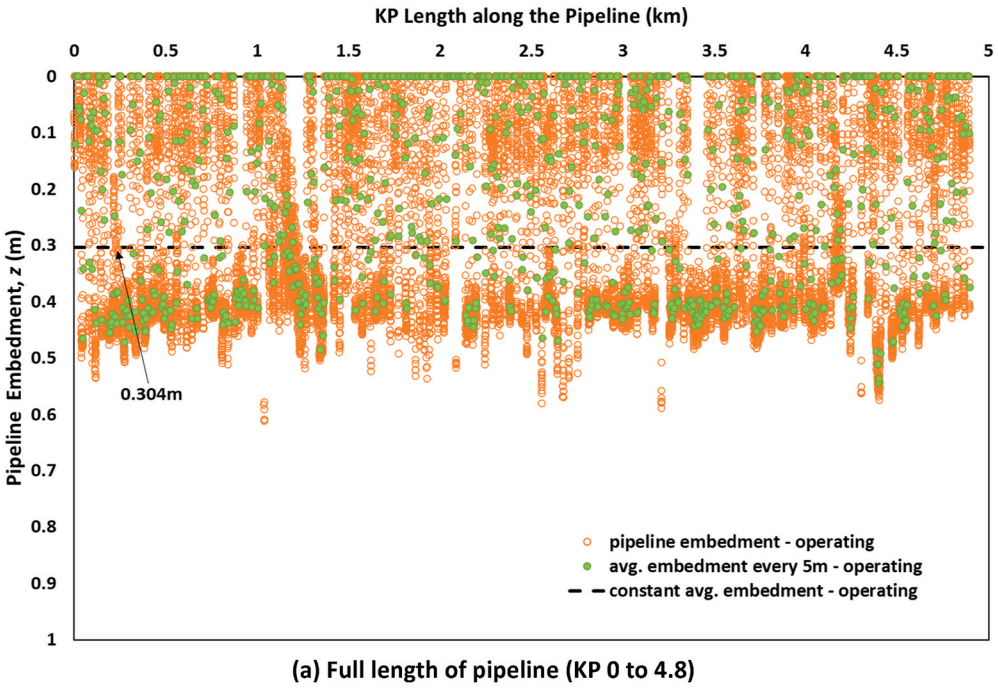

(a) Full length of pipeline (KP 0 to 4.8)

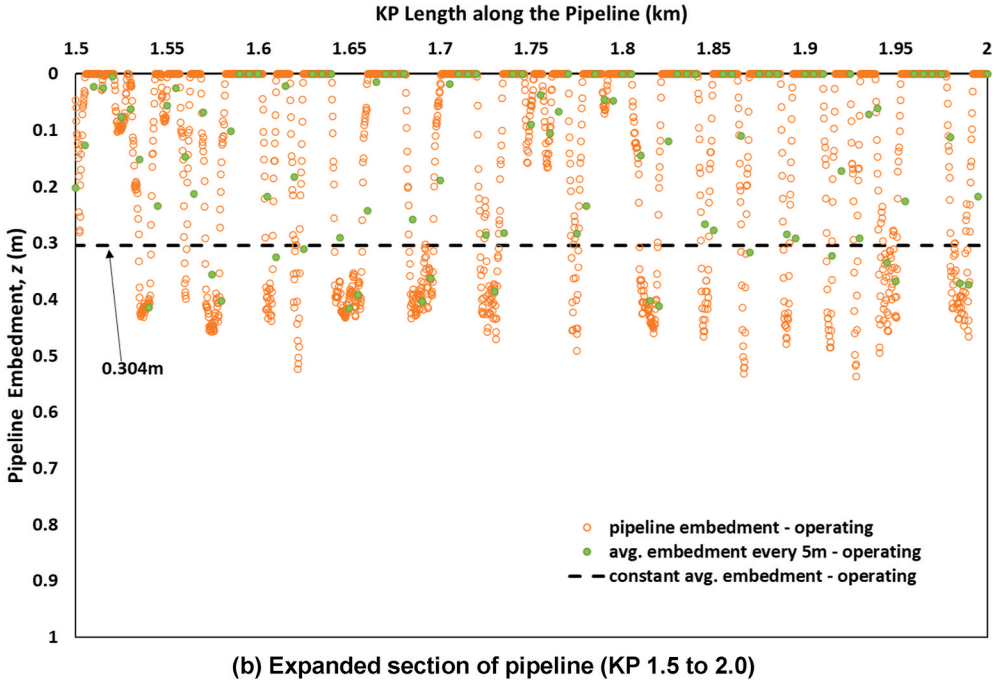

(b) Expanded section of pipeline (KP 1.5 to 2.0)

Fig. 17. Pipeline operating condition average embedment along the seabed.

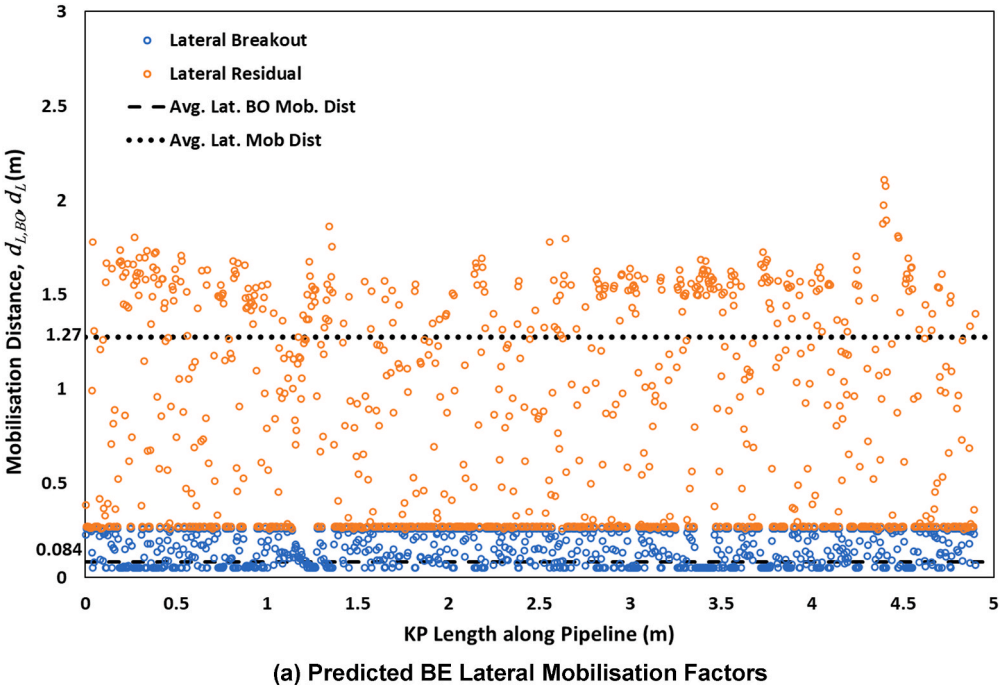

(a) Predicted BE Lateral Mobilisation Factors

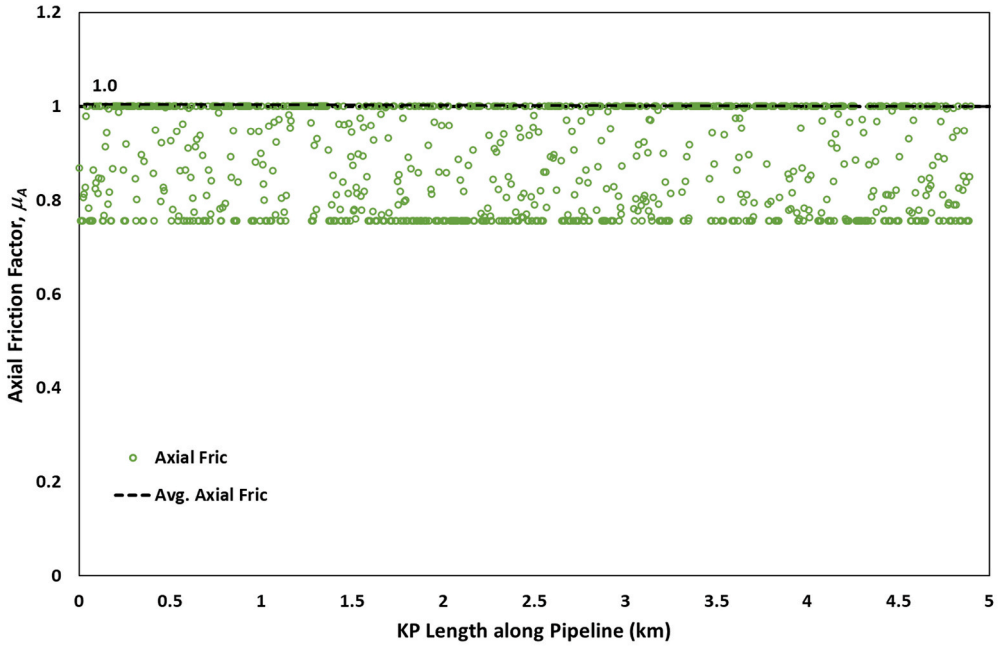

(b) Predicted BE Axial Friction Factors

Fig. 18. Predicted PSI along pipeline in post-hydrotest condition.

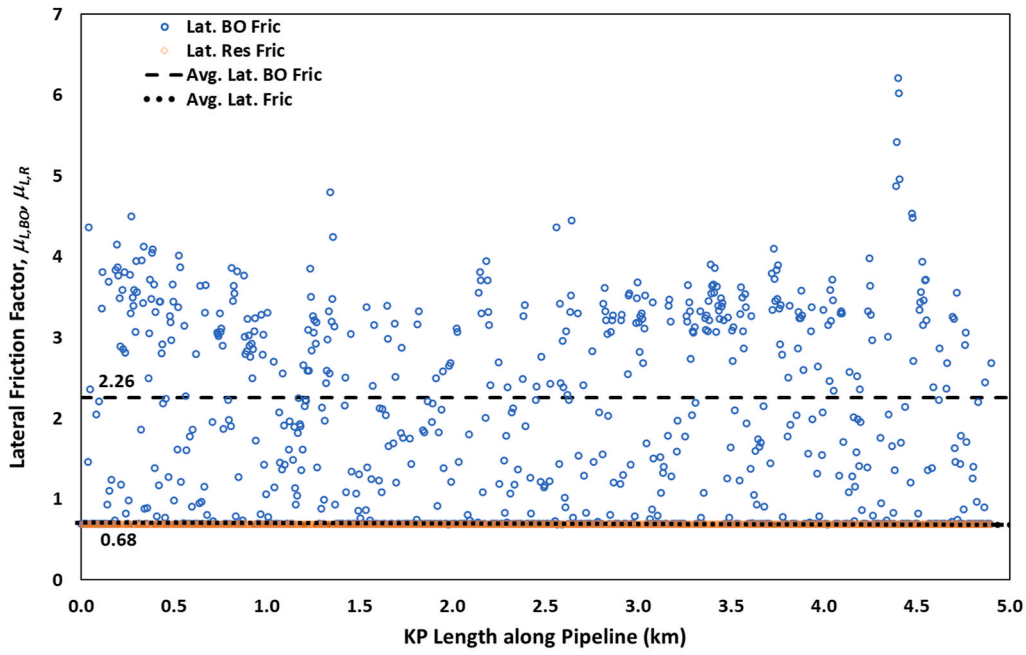

(c) Predicted BE Lateral Friction Factors

Fig. 18. (*continued*).

8. Results and discussion

This section describes simulations of the 4.8 km pre-deformed pipeline with 96m wavelength (50 sinusoidal lobes) and 10m amplitude, installed on uneven seabed and with realistic embedment. These results are compared to those for a straight pipeline (without any mitigation for lateral buckling) and a pipeline using Zero Radius Bend (ZRB) initiators, also with the realistic uneven seabed and embedment profile.

8.1. Constant BE PSI along the pipeline

The first analysis was undertaken using constant average PSI parameters along the pipeline where it is contact with the seabed, as described earlier and shown on Figs. 18 and 19. Fig. 24 shows (in plan view) the lateral position of the pre-deformed pipeline during pre-deformation, when it is first placed on the seabed prior to operation, and at the operating condition (at 140 °C and 170 bar internal pressure). The pipeline is first plastically pre-deformed at 10m amplitude – and as the bending exceeds the yield strength, plastic deformation occurs, resulting in permanent strain and deformation remained even after the pre-deformation load is removed. When the pipeline is installed on the seabed with the initial bending unloaded, the elastic part of the strain vanishes, and the remaining plastic strain represents the residual strain. This is called the 'springback' effect – due to the residual strain, the pipeline on the seabed retains some residual curvature in each lobe, with the amplitude of the deformed pipeline reduced to about 2m before increasing again to maximum of less than 3m during operating condition.

Fig. 25 shows the effective axial force in the pre-deformed pipeline showing that the pipeline forms into a series of small VAS lengths, each made up of 4–8 pre-deformation wavelengths, i.e. 400-800m long, therefore decreasing the feed-in force to each isolated section of the pipeline. Fig. 26 presents the longitudinal tensile strain of the pipeline, which decreases from 0.42% during pre-deformation to less than 0.16% when it is empty on the seabed and then during operating reaches a maximum of 0.37%.

Fig. 27 compares the lateral displacement of the pre-deformed pipeline at the operating condition of 140 °C and 170 bara with a straight pipeline on seabed assuming no initial horizontal out of straightness (HOOS). Also shown is the lateral displacement of the pipeline with 4 ZRBs, each of which has a lateral displacement between 5 and 7m from the straight alignment (the locations of the ZRBs are shown). The lobes of the pre-deformed pipeline displace laterally by less than both the straight pipeline and pipeline with ZRBs. The straight pipeline, without intervention, forms uncontrolled upheaval buckles at discrete seabed features (e.g. sand waves), with a maximum vertical displacement of 7m. Node 'A' (KP 1.01), Node 'B' (KP1.05) and Node 'C' (KP3.78) on Fig. 27 are locations of the buckles along the pipeline that are used for plotting the effective axial force variation with operating load presented in Fig. 31 for the three models.

Fig. 28 presents the effective axial force for the three cases studied, and shows that the pre-deformed pipeline reaches less than half the effective force seen by the straight pipeline without mitigation. The post-buckle axial force of the pre-deformed pipeline is also lower than the pipeline with ZRBs. The straight pipeline formed 5 upheaval buckles, and therefore formed 5 VAS lengths while the pipeline with 4 ZRBs buckled at the ZRB locations, forming 4 VAS lengths. In contrast, the pre-deformed pipeline developed 9 (small) VAS lengths naturally at locations where the effective axial force and feed-in were shared. This process limits feed-in to each buckle – which are formed by expansion of the pre-deformation lobes – leading to lower longitudinal strain than the straight pipeline and pipeline with ZRBs.

Fig. 29 compares the longitudinal tensile strain for the three cases. The maximum strain of the straight pipeline due to upheaval buckling is 0.49%, whereas the maximum strain for pipeline using 4 ZRBs to control buckling is 0.40% and the maximum strain for the pre-deformed pipeline is 0.37%. This clearly shows that the PDP achieves lower strain levels than the solution using ZRBs for lateral buckling control.

Fig. 30 presents the axial displacement for the three cases studied. The axial displacement at the pipeline ends (also called pipeline end expansion) is an important input to design of tie-in spools or other termination structures design – the higher the end expansion, the greater the need to accommodate pipeline end expansion in order to minimize stress to the connecting structures.

As shown in Fig. 30 the pre-deformed pipeline had the lowest end expansion, equal to 0.38m at the pipeline inlet (KP 0) and 0.61m at the

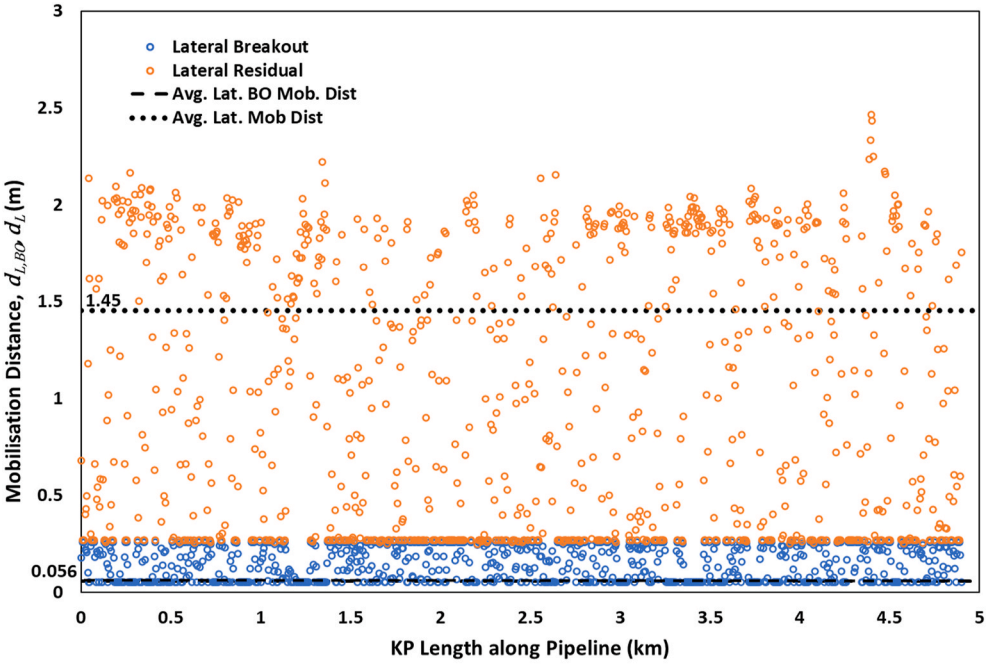

(a) Predicted BE Lateral Mobilisation Factors

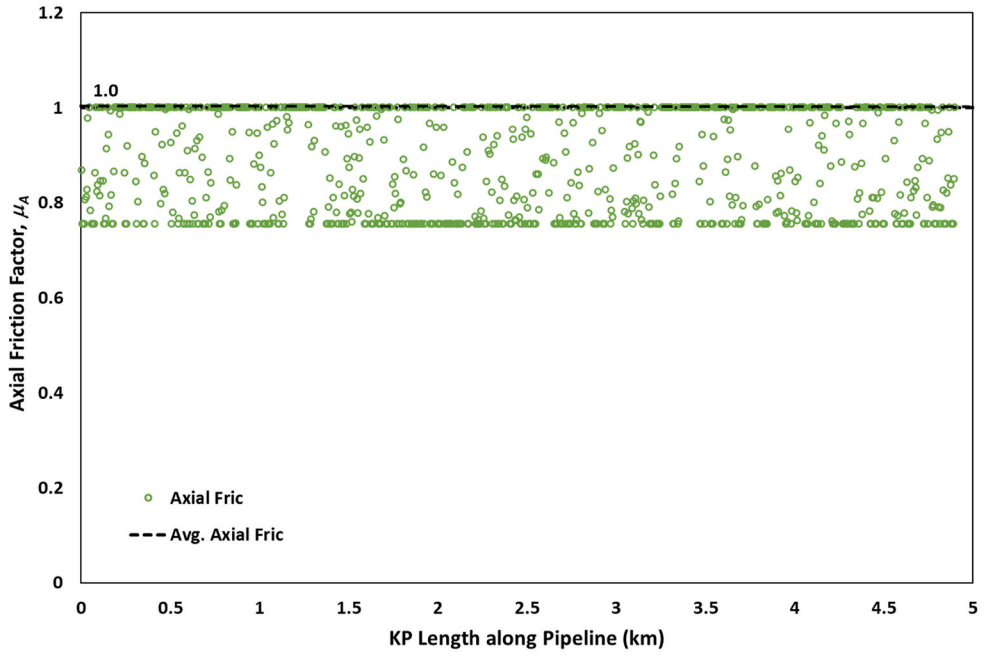

(b) Predicted BE Axial Friction Factors

Fig. 19. Predicted PSI along pipeline in operating condition.

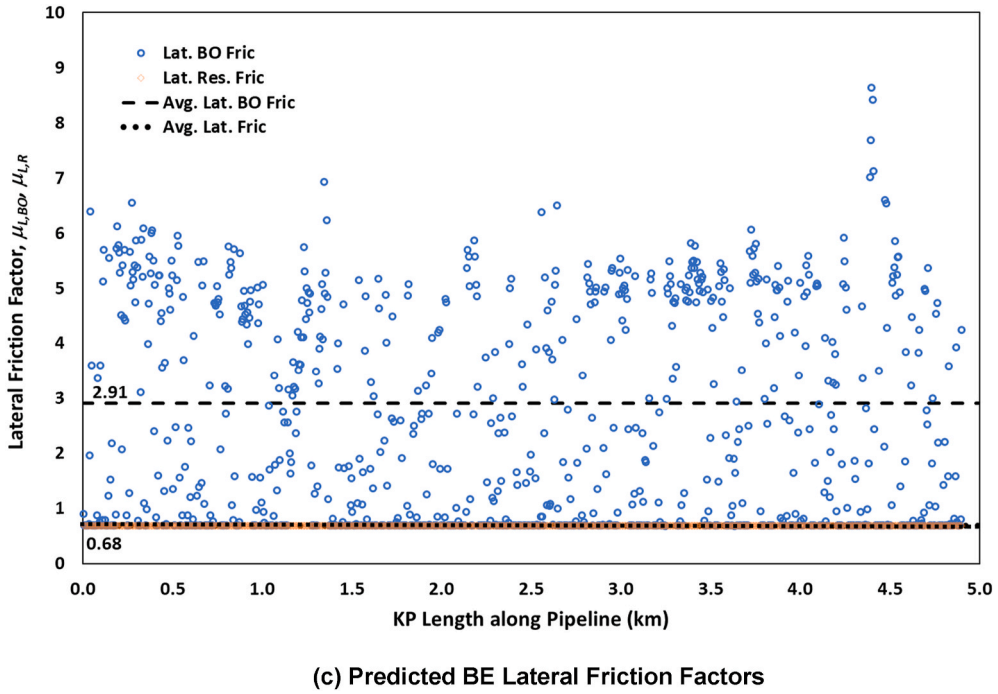

Fig. 19. (*continued*).

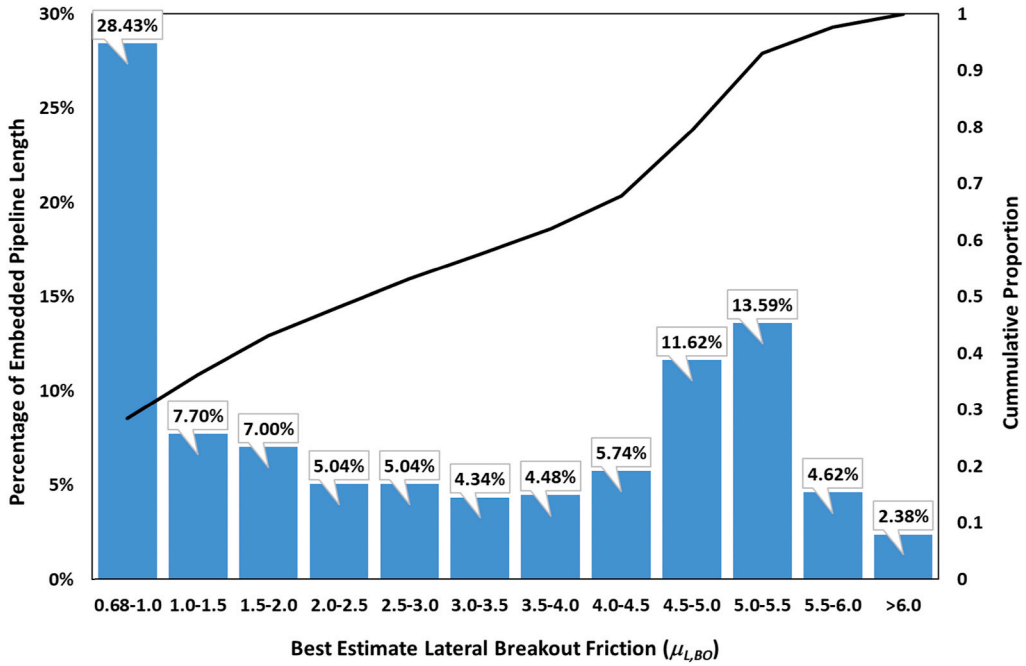

Fig. 20. Statistical data of the operating lateral breakout friction factor.

pipeline outlet (KP 4.8). The inlet and outlet axial displacement of the pipeline with ZRBs was 0.82m and 0.91m respectively, while for the straight pipeline, the axial displacement at the inlet is 0.95m and 1.39m at the outlet. Note that while the pressure and temperature applied is constant along the pipeline, the variable PSI and buckle locations leads to different axial displacement at each end. The pre-deformed pipeline has formed more VAS lengths along the pipeline, therefore minimizing end expansion of the pipeline.

Finally, the effective axial force against operating temperature is plotted and shown in Fig. 31. The locations where the effective axial force variation was taken are Nodes 'A' (KP 1.01 of the pre-deformed pipeline), 'B' (KP 1.05 of the pipeline with ZRBs) and 'C' (KP 3.78 of the straight pipeline), which are marked on Figs. 27 and 28 and 29. These represent the buckle locations with the lowest initiation force (for each case). The pipeline with ZRBs buckled at 39.4 °C and the straight pipeline buckled at 34.1 °C, while the pre-deformed pipeline buckled at 52.7 °C. Both the straight pipeline with ZRBs and the pre-deformed pipeline formed stable buckles, whereby the effective axial force did not have a sudden drop when temperature and pressure is increased; while the straight pipeline without any mitigation exhibited snap-through buckling behaviour that cause a high strain.

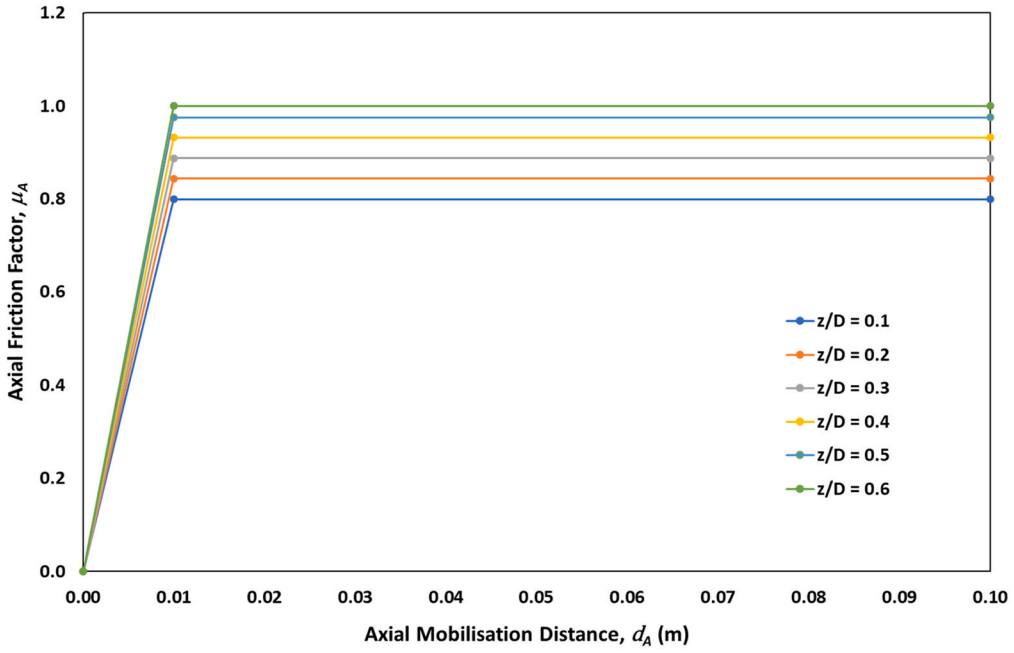

(a) Predicted BE Axial Friction Factors against Axial Mobilisation Distance

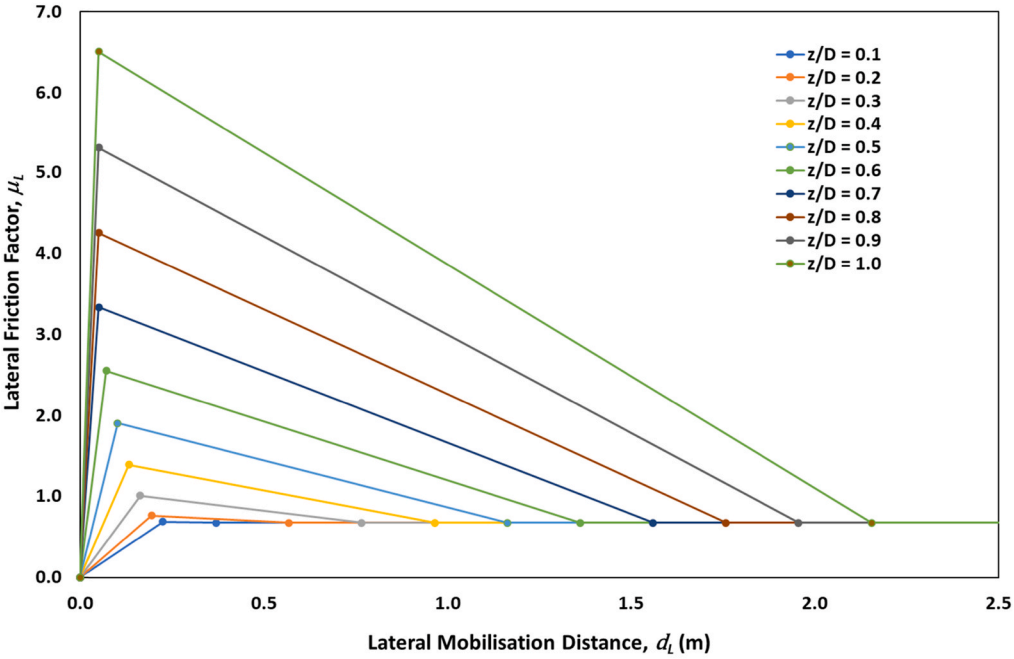

(b) Predicted BE Lateral Friction Factors against Axial Mobilisation Distance

Fig. 21. Predicted friction factors against mobilisation distance in operating condition.

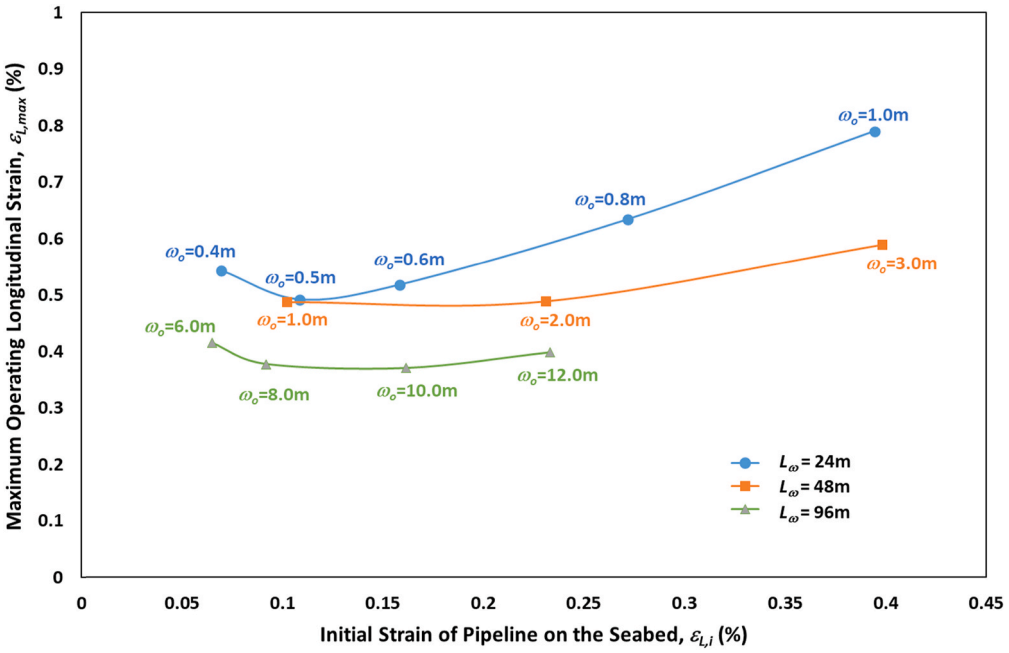

Fig. 22. Maximum strain in pre-deformed pipeline at operating condition for different pre-deformed Configurations.

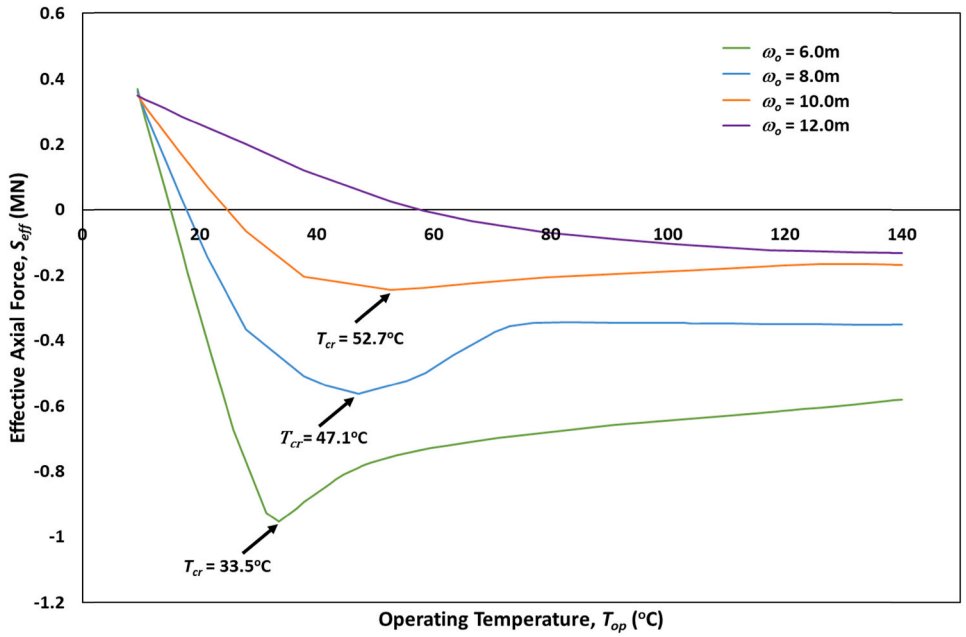

Fig. 23. Effective axial force against applied temperature (L_ω = 96m).

8.2. *Variable BE PSI along pipeline*

The previous analysis was undertaken for constant (average) PSI parameters along the pipeline where it is contact with the seabed, as described earlier and shown on Figs. 18 and 19. To examine the sensitivity of the analysis to the local variations in embedment and the resulting PSI input parameters, the analysis was repeated with PSI inputs that vary accordingly to the surveyed embedment along the pipeline (also shown on Figs. 18 and 19). Figs. 32–35 show the lateral displacement, effective axial force, longitudinal strain and axial displacement of the straight pipeline, pipeline with four ZRBs and pre-deformed pipeline. The effective axial force against operating temperature for the variable PSI case is shown in Fig. 36. The location and lateral displacement of the straight pipeline and pipeline with ZRBs is similar to the respective cases using the constant average PSI. This occurs because the buckle locations – with upheaval buckling for the straight pipeline, and lateral buckling for the pipeline with ZRBs – occur where the pipeline is not in contact with the seabed, so the PSI inputs do not significantly affect the results.

In contrast, the lateral displacement for the pre-deformed pipeline differs slightly from the case of constant PSI input, reflecting differences in embedment and therefore PSI resistance at different lobes, as illustrated by the calculated profiles of PSI resistance with KP shown earlier. This influence of PSI is particularly linked to the effect of embedment on breakout resistance, which influences the shape of the lobes during thermal loading, with similar findings reported by Wang and Van Der

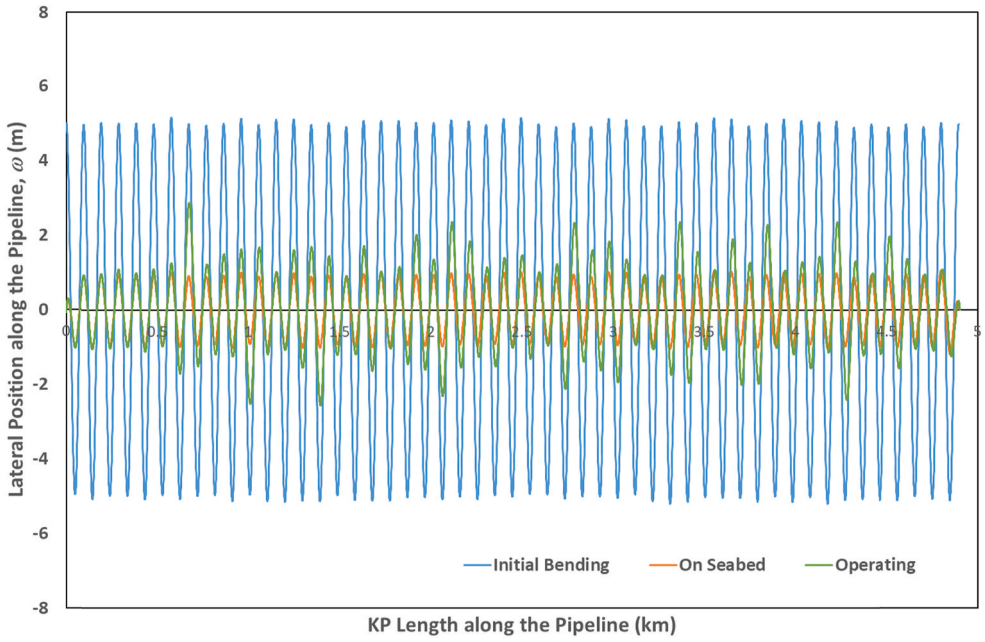

Fig. 24. Lateral deflection of the pre-deformed pipeline.

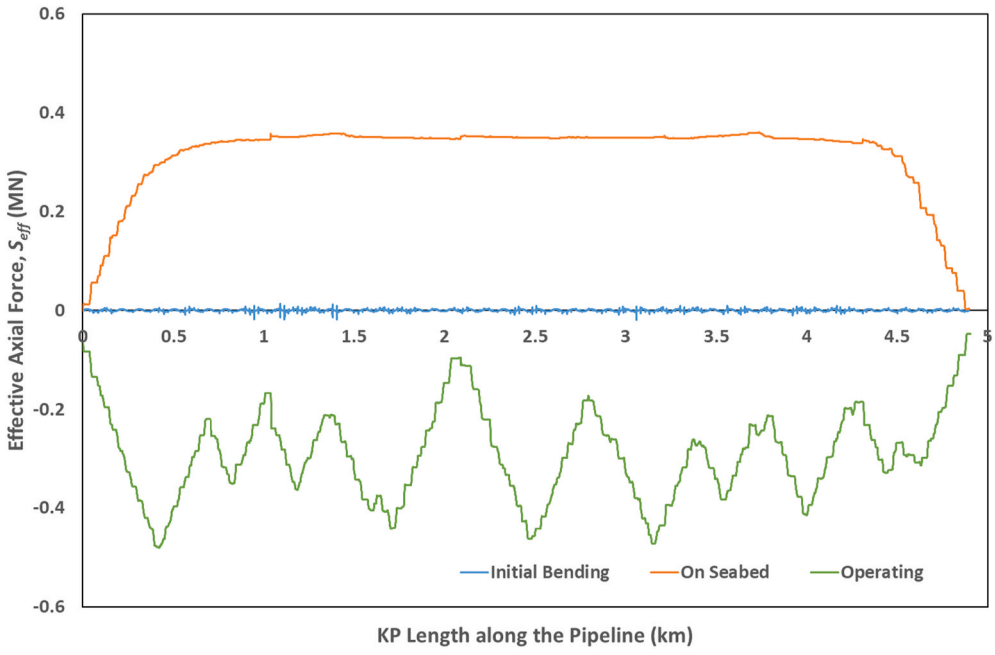

Fig. 25. Effective axial force of pre-deformed pipeline.

Heijden (2017)However, while the shape is affected by the variable PSI input along the pipeline, the pre-deformed lobes simply reshuffle and again form multiple small VAS lengths, as shown by comparisons between the PDP cases with constant and variable PSI in Figs. 37–39 and 40. The end result in terms of maximum and average strain in the pipeline is similar for the case of a pre-deformed pipeline, which again shows lower (0.39%) maximum tensile strain than either the straight pipeline (0.49%) of the pipeline with ZRBs (0.44%). Similar to the cases with constant PSI, the pre-deformed pipeline with variable PSI still shows the lowest end expansion compared to the pipeline with ZRBs and straight pipeline with axial displacement of 0.35m at the inlet end and 0.69m at the outlet end. The buckle initiation force histories also remain similar between constant and variable PSI input analysis as shown in Fig. 41.

Further evidence of the robustness of the pre-deformed pipeline is shown by two additional cases that were analysed - using a constant value of low estimate (LE) and high estimate (HE) lateral friction factors along the pipeline, respectively. The constant BE resistance was calculated as the average from the variable profile linked to the embedment (as marked on Fig. 19(c)). The LE and HE cases represent the uncertainty associated with the pipe-seabed interaction forces due to uncertainty in the underlying geotechnical parameters and calculation methods. For simplicity, the LE and HE values were calculated by increasing and decreasing both the lateral breakout and residual BE friction factors by 50%, which is approximately consistent with the range found in the case study design PSI parameters. These parameters were determined using

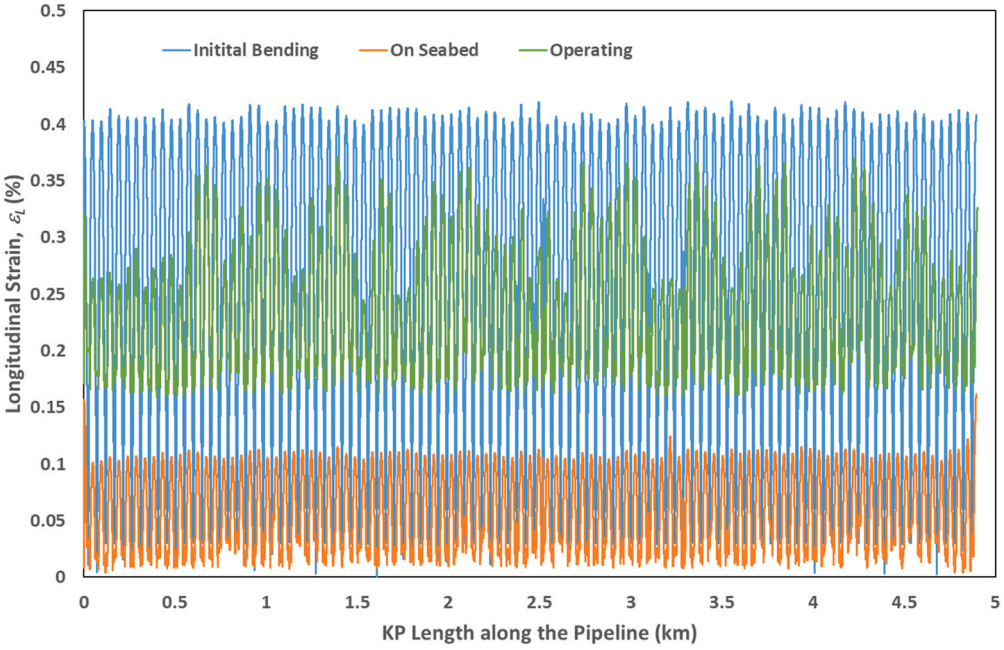

Fig. 26. Longitudinal tensile strain of pre-deformed pipeline.

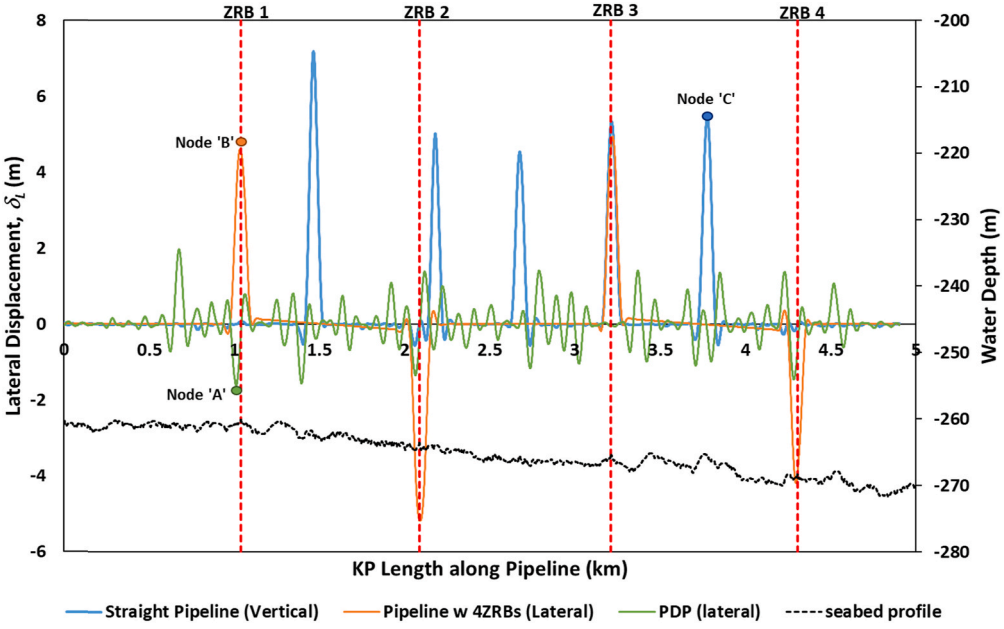

Fig. 27. Lateral Displacement at the end of Operating Condition (140 °C, 170 bar).

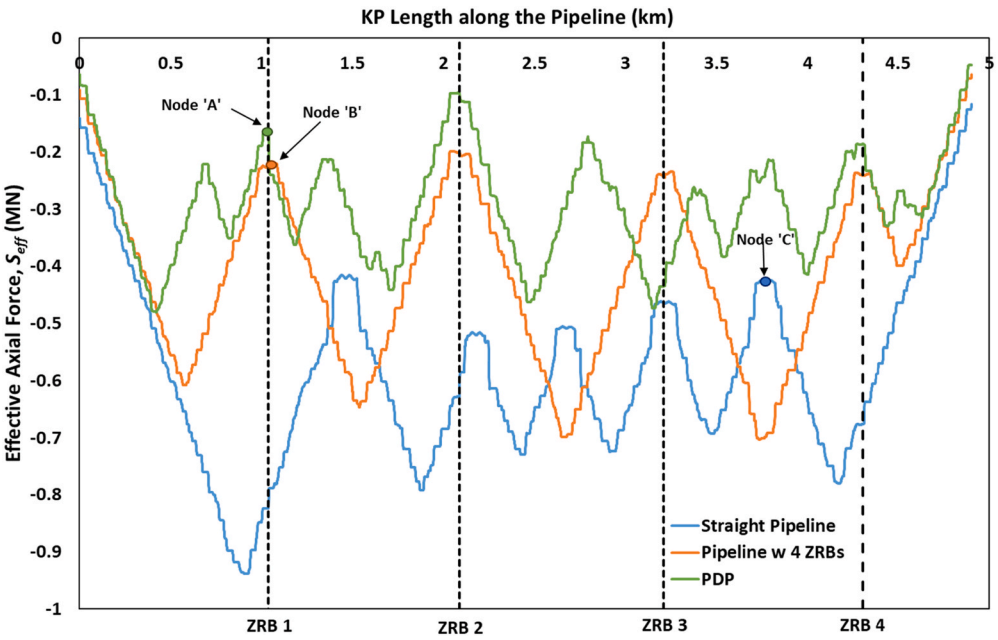

Fig. 28. Effective axial force at the end of operating condition (140 °C, 170 bar).

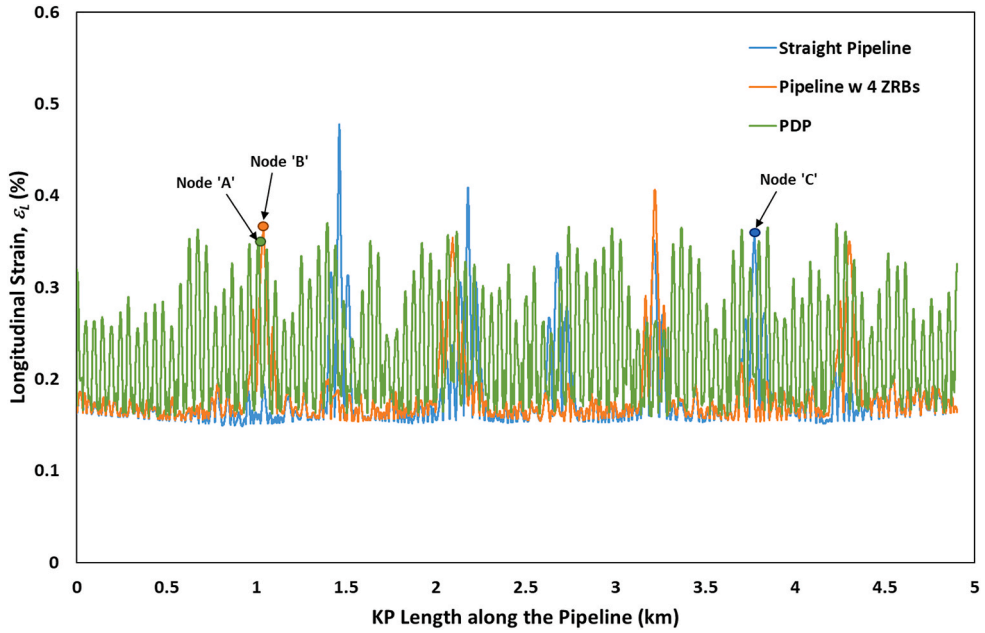

Fig. 29. Longitudinal Tensile Strain at the end of Operating Condition (140 °C, 170 bar).

industry best practice, following a Monte Carlo treatment of the geotechnical parameter and model uncertainty (e.g. White et al., 2015).

Results summarised in Fig. 42 show that the maximum longitudinal strain in the pre-deformed pipeline is largely unaffected by changes in the PSI parameters between the LE, BE and HE values. This is due to the pre-deformed pipeline geometrically rearranging itself to minimize the strain levels as shown in Fig. 43. While the straight pipeline did not show any difference in response (reflecting the formation of upheaval buckles, which are unaffected by PSI), the longitudinal strain for the pipeline with ZRBs increased from 0.35% to 0.43% as the lateral soil friction increased from LE to HE. Overall, this provides confidence that the pre-deformed pipeline method is robust, and the resulting strain does not significantly change with the lateral soil PSI.

9. Conclusion

This study confirms the value of a novel approach to control the thermal and pressure-induced lateral buckling of subsea pipelines using the method of pre-deforming the pipeline into a continuous wavy profile. A case study of an existing in-field pipeline is created using embedment profile data and seabed bathymetry for this site on the North West Shelf, Australia. The response of the pre-deformed pipeline to hydrotesting and loading by temperature and pressure to the operating condition is compared with the adopted method of controlling lateral buckling for this pipeline, which utilized Zero Radius Bend (ZRB) structures at specific locations along the pipeline route. A straight pipeline without any lateral buckling control or mitigation method is also analysed for comparison. These three models were analysed with

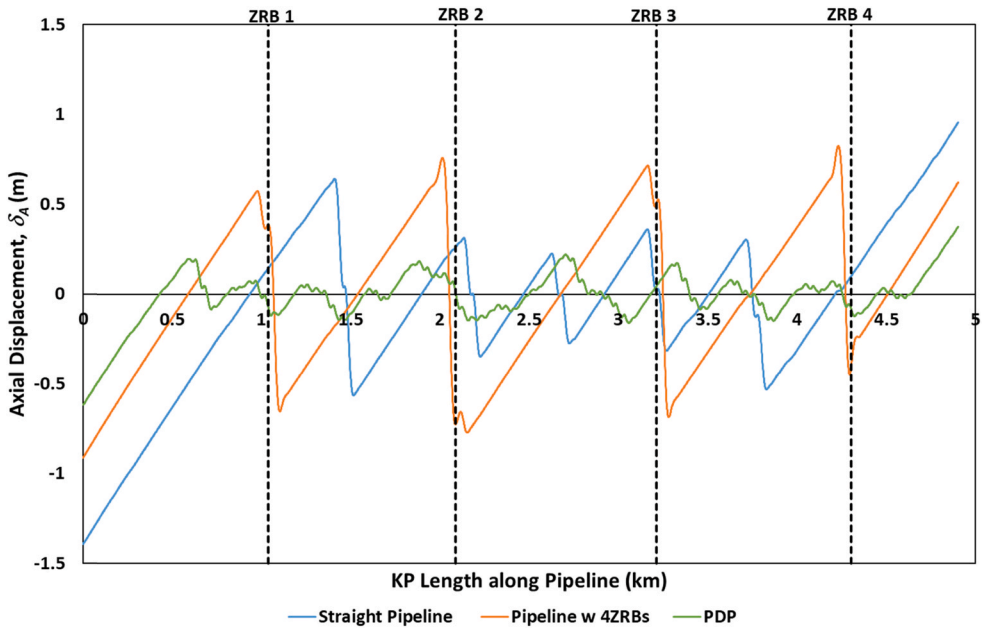

Fig. 30. Axial Displacement at the end of Operating Condition (140 °C, 170 bara).

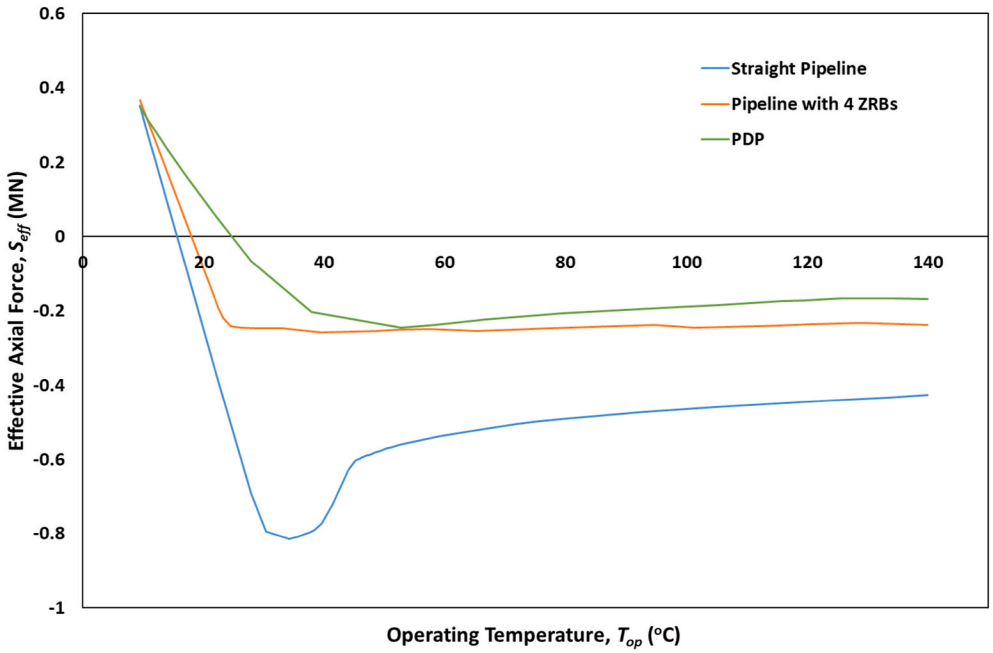

Fig. 31. Time history of effective axial force at operating temperatures.

two different PSI scenarios: (i) constant PSI parameters along the pipeline and (ii) variable PSI parameters along the pipeline, based on the surveyed embedment data.

The pre-deformed pipeline has lower axial stiffness than a straight pipeline, and therefore has a reduced tendency to buckle when heated. Using analytical calculations, the axial stiffness of the pre-deformed pipeline for several different and pre-deformation wavelengths and amplitudes was investigated and a selected design solution of 96m wavelengths proved to have the lowest axial stiffness with minimal sensitivity to the achieved deformation amplitude. Numerical modelling was then employed to determine the lowest final longitudinal strain along the pipe at these operating conditions on the realistic uneven seabed. It was shown that the pre-deformed pipeline had lower strain than the ZRB and straight pipeline options, for both PSI conditions.

From this comparative study, the following specific conclusions can be drawn.

1. The straight pipeline without any mitigation method against thermal expansion developed upheaval buckling triggered by the vertical undulations of the seabed, which had an amplitude of 4–5m, while the pipeline with ZRBs buckled at the 4 locations of the ZRBs. The pre-deformed pipeline simply formed a series of short VAS lengths and the pre-deformed lobes expanded slightly in the lateral direction with a maximum displacement of 2m compared to 5–7m for the pipeline with ZRBs.

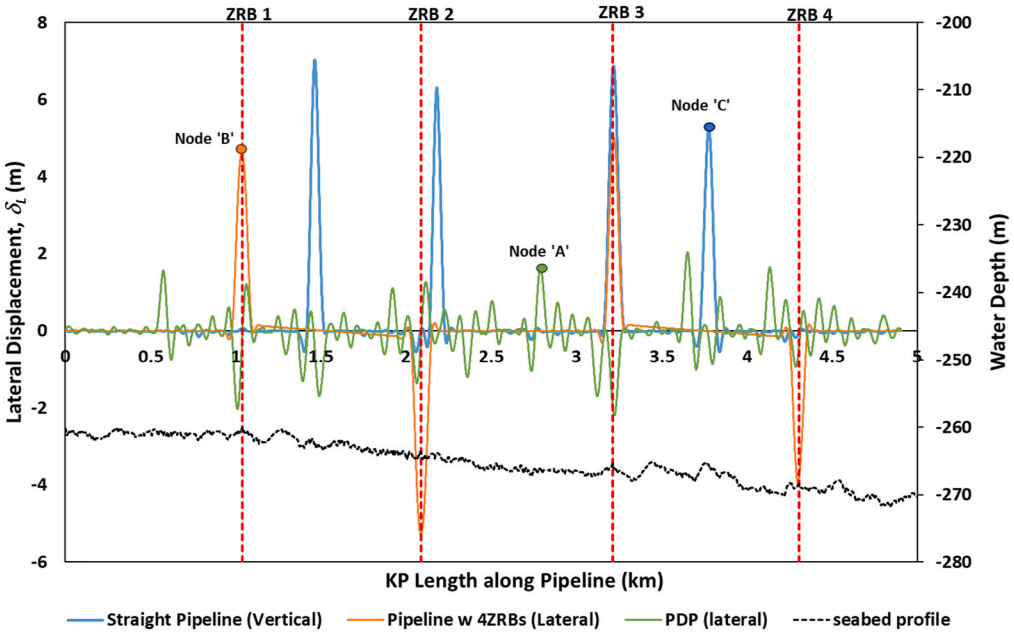

Fig. 32. Lateral Displacement at the end of Operating Condition (140 °C, 170 bar, variable PSI).

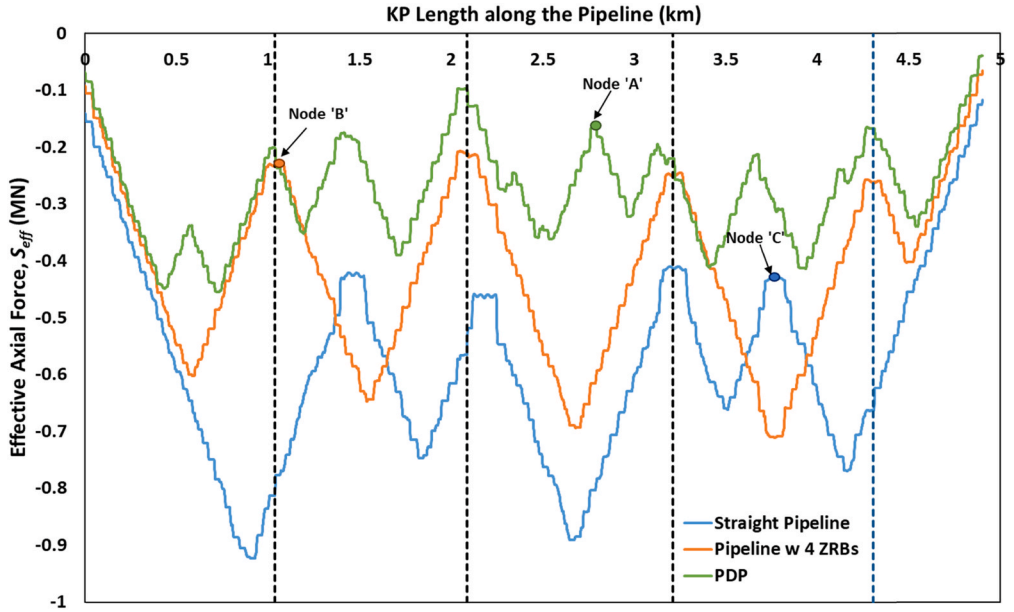

Fig. 33. Effective Axial Force at the end of Operating Condition (140 °C, 170 bar, variable PSI).

2. The final maximum longitudinal tensile strain is greatest for the pipeline without mitigation at 0.49%, followed by the pipeline with ZRBs of 0.40%. The pre-deformed pipeline is the best solution, with a strain of 0.37%. This lower strain, when considered as a cyclic range during operating cycles, translates into a greater fatigue life.
3. Increasing the lateral soil friction factors from LE to HE did not have significant impact on the resulting maximum strain in the pre-deformed pipeline, which only varied between 0.37 and 0.38%. The straight pipeline without mitigation remained at 0.49% regardless of the change in lateral PSI as it buckles in an upheaval mode. However, the longitudinal strain for the pipeline with ZRBs increased from 0.35% to 0.44% when the lateral PSI increase from the LE to HE values.
4. In these analyses, the adoption of variable PSI parameters along the pipeline length linked to the observed embedment profile did not change in the deformation pattern for the straight pipeline and the ZRB case.
5. In the case of the pre-deformed pipeline, the modelling of PSI parameters that varied with embedment led to a change to the pattern of lobe expansions, with the expansion being reshuffled along the pipeline, leading to the formation of different short VAS lengths. However, the maximum strain remained the lowest among the 3 cases.
6. The pipeline end expansion for the pre-deformed pipeline is the lowest compared to the pipeline with ZRBs and the straight pipeline without mitigation, reducing the severity of the end expansion needed to be tolerated by the connecting termination structures or spools.

In summary, it is shown by this analysis that the pre-deformation

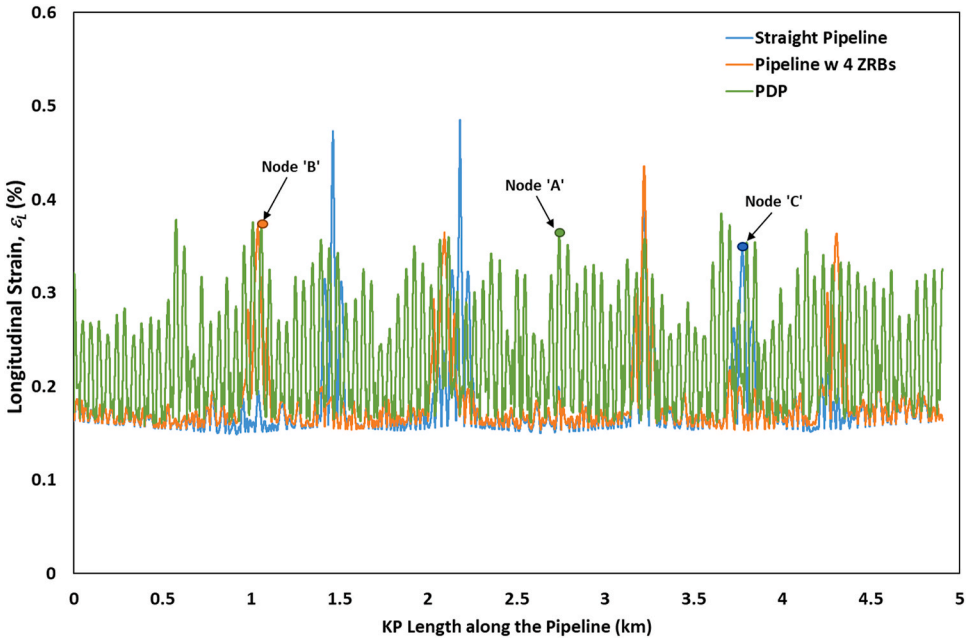

Fig. 34. Longitudinal Tensile Strain at the end of Operating Condition (140 °C, 170 bar, variable PSI).

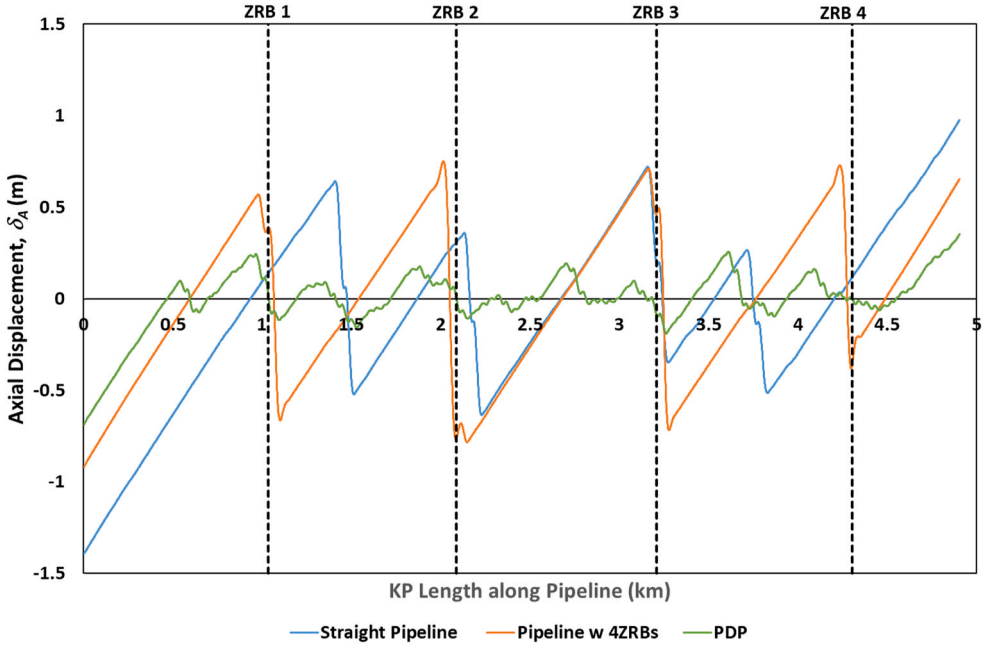

Fig. 35. Axial Displacement at the end of Operating Condition (140 °C, 170 bar, variable PSI).

method is highly robust. The pipeline is able to adjust itself by geometric rearrangement to minimize the strain levels created by operation at high pressure and temperature. It effectively creates a series of short pipelines, each with minimal expansion to absorb and therefore reduce the strain level. The PDP approach enables the pipeline to be installed and operated safely at very high temperatures without the need for the design and installation of expensive structures such as buckle initiators. The PDP approach also mitigates against post-installation issues such as excessive pipe spans and seabed scours, because the entire length of pipeline is available to locally absorb any additional expansion strain. The PDP approach is therefore a valuable alternative tool for the subsea pipeline industry, which offers potential cost savings and improved pipeline system reliability.

CRediT authorship contribution statement

Jayden Chee: Writing – original draft, Methodology, Investigation, Formal analysis, Data curation, Conceptualization. **Phil Watson:** Writing – review & editing, Validation, Supervision, Project administration, Methodology, Funding acquisition, Data curation, Conceptualization. **David White:** Writing – review & editing, Validation, Supervision, Methodology, Data curation, Conceptualization. **Alastair Walker:** Writing – review & editing, Supervision.

Declaration of competing interest

The authors declare that they have no known competing financial

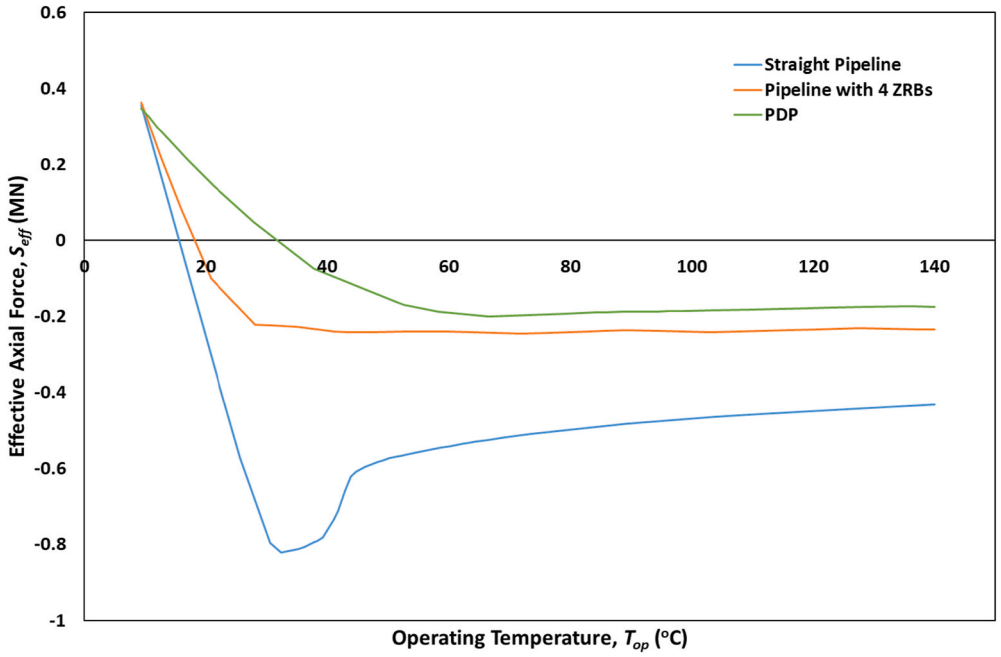

Fig. 36. Time history of effective axial force (variable PSI).

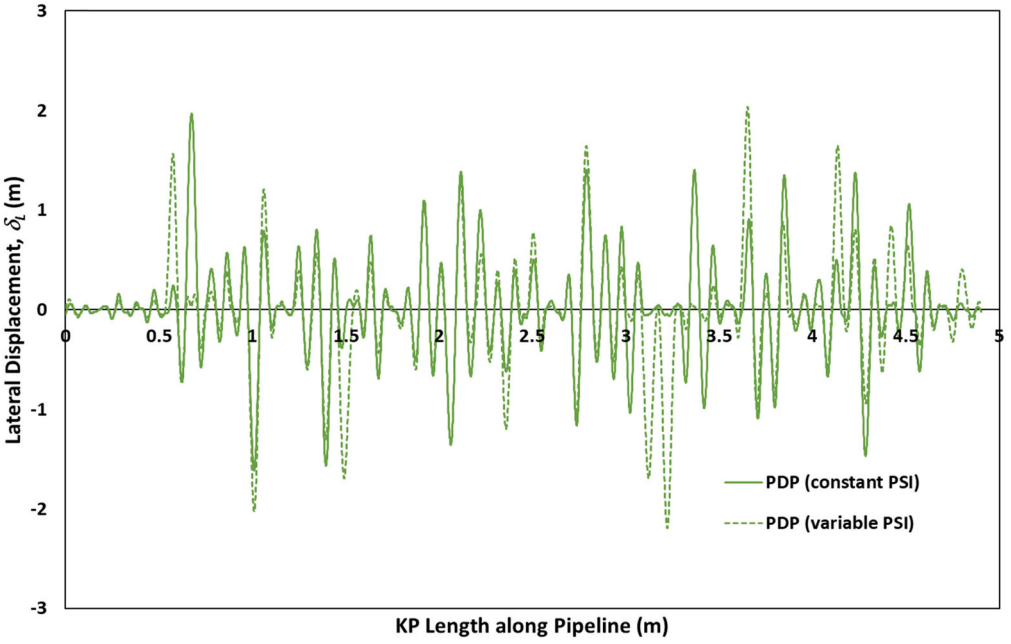

Fig. 37. Lateral Displacement at the end of Operating Condition (140 °C, 170 bar) for PDP.

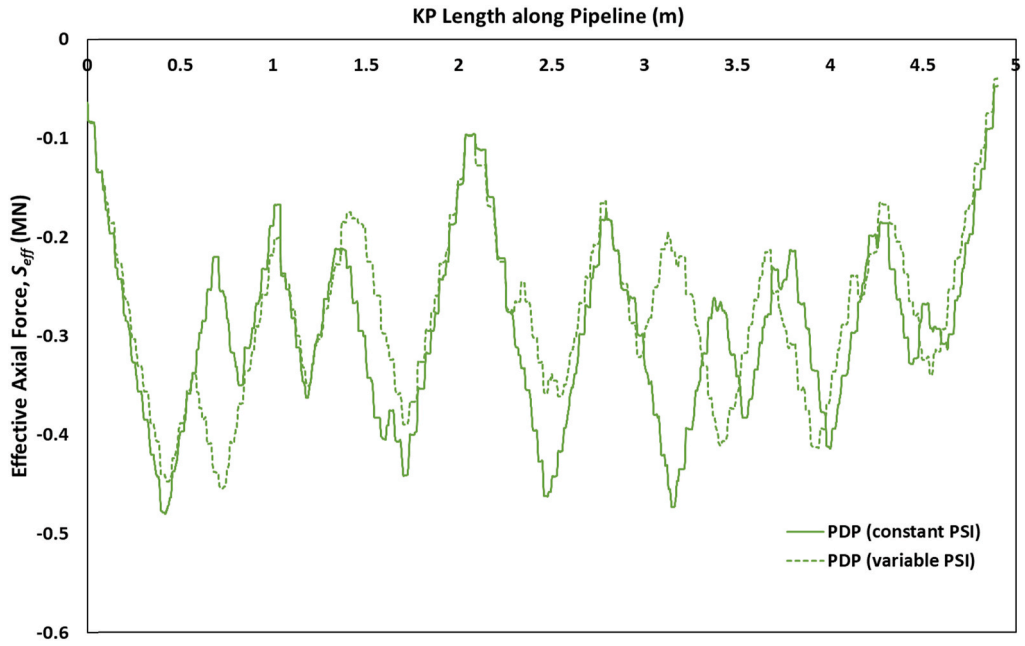

Fig. 38. Effective Axial Force at the end of Operating Condition (140 °C, 170 bar) for PDP.

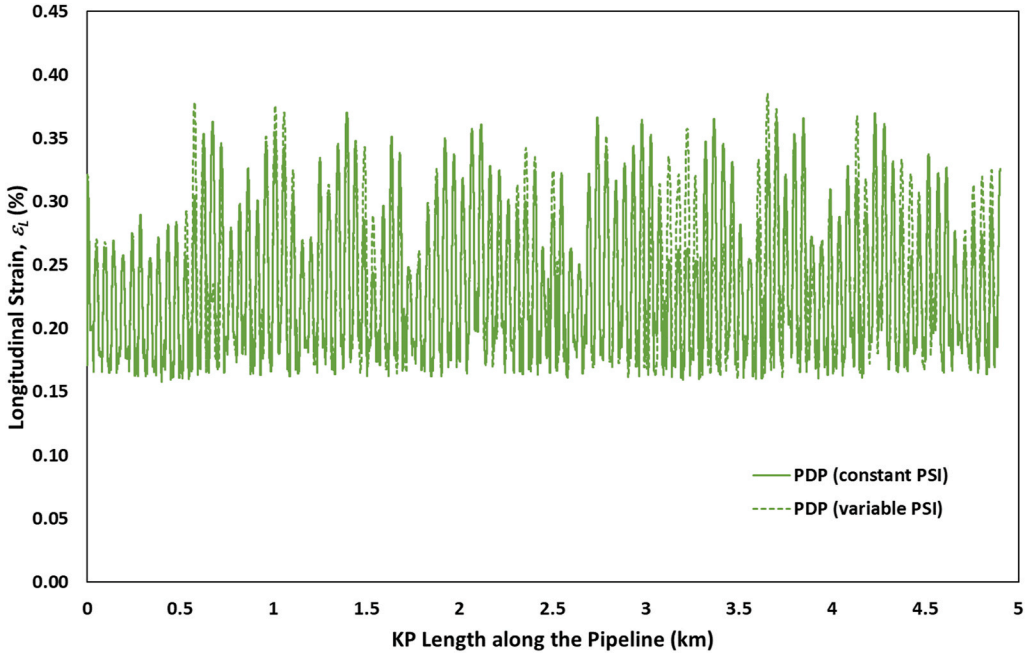

Fig. 39. Longitudinal Strain at the end of Operating Condition (140 °C, 170 bar) for PDP.

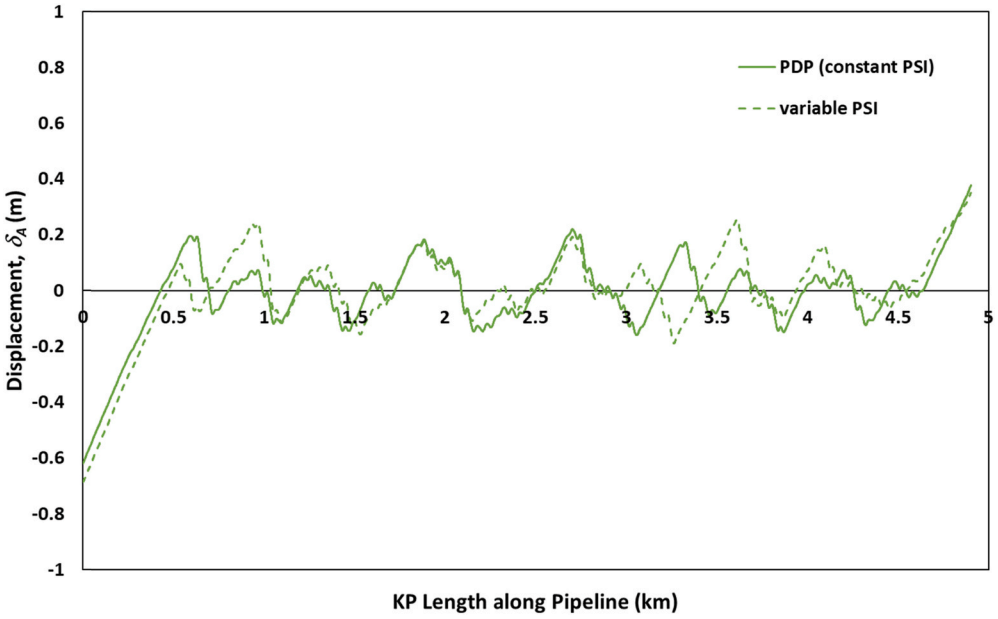

Fig. 40. Axial Displacement at the end of Operating Condition (140 °C, 170 bar) for PDP.

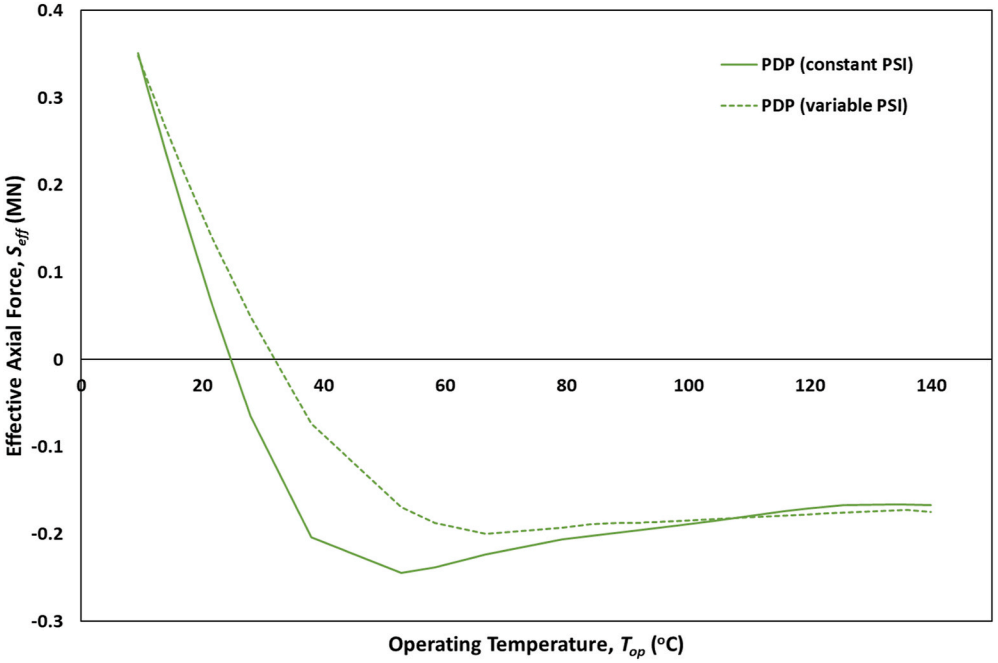

Fig. 41. Time history of effective axial force of the PDP

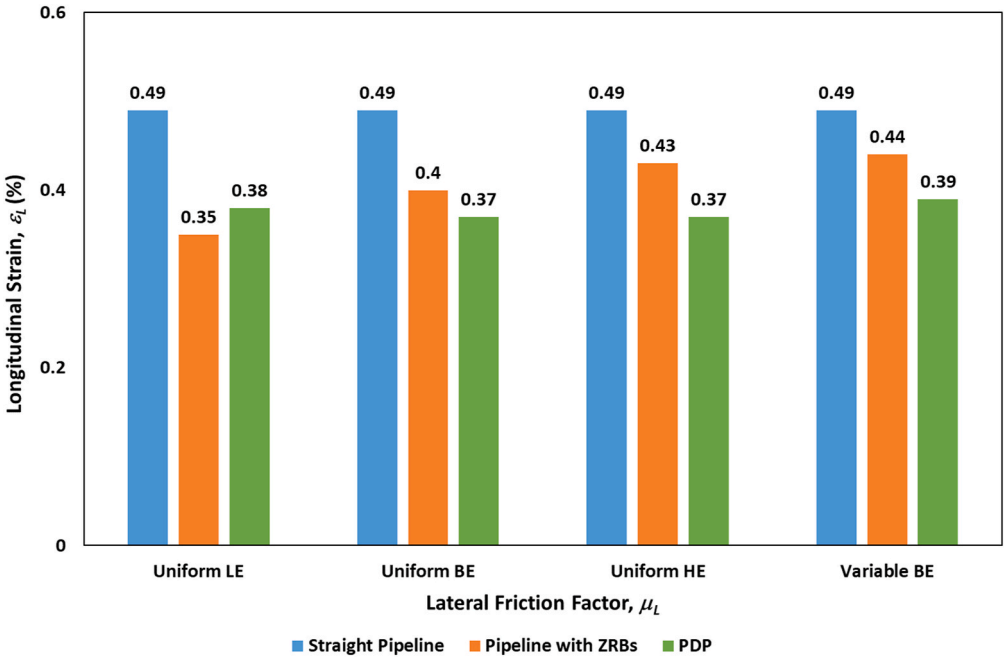

Fig. 42. Longitudinal Tensile Strain at the end of Operating Condition (140 °C, 170 bar) for different lateral PSI.

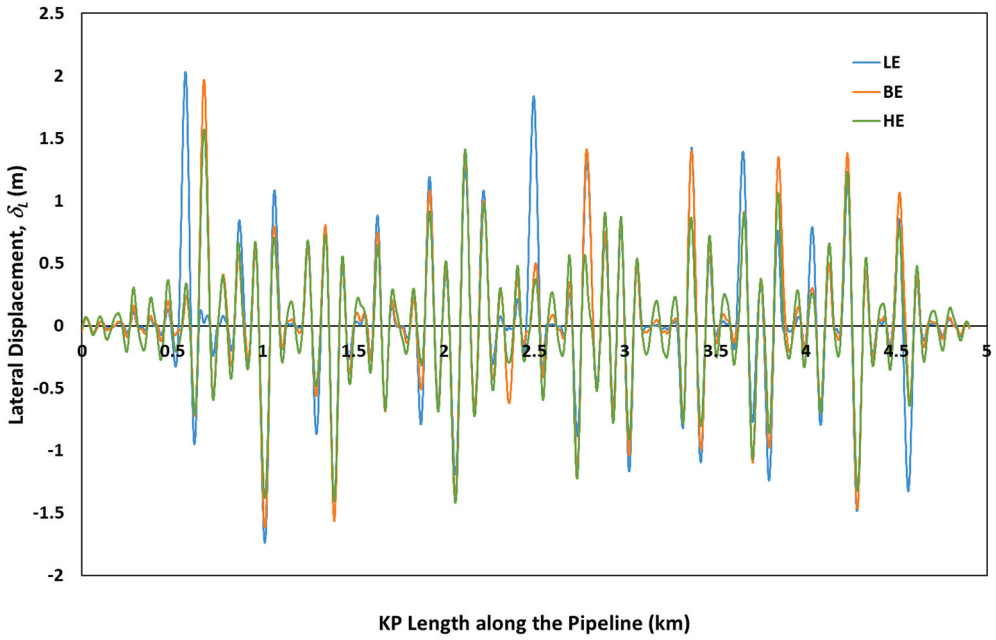

Fig. 43. Lateral Displacement at the end of Operating Condition (140 °C, 170 bar) for PDP with different lateral PSI.

interests or personal relationships that could have appeared to influence the work reported in this paper.

Acknowledgement

This work was supported by the ARC Industrial Transformation Research Hub for Transforming Energy Infrastructure through Digital Engineering (TIDE) which is funded by the Australia Research Council, INPEX, Woodside Energy, Shell, Bureau Veritas, Lloyds Register, Fugro, Wood, RPS Group, the Australian Institute of Marine Science and the Bureau of Meteorology (Grant No. IH200100009). The second author leads the Shell Chair in Offshore Engineering research team at The University of Western Australia, which is sponsored by Shell Australia – and which provides funding to the lead author.

Abbreviations

FEA	Finite Modelling Analysis
HPHT	High Pressure High Temperature
KP	Kilometer Point
OD	Outer Diameter
Op	Operating
PDP	Pre-Deformed Pipeline
PSI	Pipe-Soil Interaction
VAS	Virtual Anchor Spacing
WD	Water Depth

WT	Wall Thickness
ZRB	Zero Radius Bend

References

Abaqus Analysis User Manual, 2020. Abaqus Version 2020. Dassault Systemes.

Bahrum, B., Hamdan, H., Madsen, A., Bedrossian, A., 2023. Challenges in designing residual curvature method on large size flowline. The 33rd International Ocean and Polar Engineering Conference. Ottawa, Canada. ISOPE-I-23-220.

Chee, J., Walker, A., White, D., 2018. Controlling lateral buckling of subsea pipeline with sinusoidal shape pre-deformation. J. Ocean Eng. 151, 170–190. https://doi.org/10.1016/j.oceaneng.2018.01.024.

Chee, J., Walker, A., White, D., 2019. Effects of variability in lateral pipe-soil interaction and pipe initial out-of-straightness on controlled lateral buckling of pre-deformed pipeline. J. Ocean Eng. 182, 283–304. https://doi.org/10.1016/j.oceaneng.2019.04.034.

Cooper, P., Zhao, T., Kortekaas, F., 2017. Residual curvature method for lateral buckling of deepwater flowlines. Offshore Pipeline Technology Conference. Amsterdam, Netherlands.

Det Norske Veritas, 2021. DNV RP F110 Global buckling of Submarine Pipeline.

Endal, G., Giske, S.R., Moen, K., Sande, S., 2014. Reel-lay method to control global pipeline buckling under operating loads. Proceedings of the ASME 33rd International Conference on Ocean, Offshore and Artic Engineering. https://doi.org/10.1115/OMAE2014-24062. San Francisco, California, USA.

Endal, G., Nystrom, P.R., 2015. Benefits of generating pipeline local residual curvature during reel and S-lay installation. Offshore Pipeline Technology Conference. Amsterdam, The Netherlands.

Hou, Z., Bransby, F., Watson, P., White, D., Low, H.E., Rathbone, A., 2023. Operational integrity of pipelines on mobile seabeds: using survey data to explore trends of changing pipeline embedment and span evolution. In: Proceedings of the 9th International Offshore Site Investigation and Geotechnics Conference: Innovative Geotechnologies for Energy Transition, 1, pp. 563–572. https://doi.org/10.3723/VPFW4060, 8 pp. (Offshore Site Investigation and Geotechnics).

Lanan, G.A., Barry, D.W., 1992. Mobile bay fairway field flowline project. Offshore Technology Conference. Houstan, Texas, USA.

Mamoon, A., Zhao, M., Wu, H., Keshavarzi, A., Hu, P., An, H., 2023. Local scour around a pipeline sleeper system under different flow directions. Coast Eng. 183, 104335.

Peek, R., Kristiansen, N., 2009. Zero-radius bend method to trigger lateral buckles. J. Transport. Eng. 135 (12), 946–952. https://doi.org/10.1061/(ASCE)TE.1943-5436.0000076.

Powell, T.J., Bai, Q., Brunner, M., Searle, S., 2019. Challenges of using residual curvature method in deep water pipelines. Proceedings of the 24th Offshore Symposium. The Society of Naval Architects and Marine Engineers, Houston, Texas.

Rodriguez, A.B., Bransby, M.F., Finnie, I., Low, H.E., White, D.J., 2013. Changes in pipeline embedment due to sediment mobility: observations and implications for design. Proceedings of the ASME 2013 32nd International Conference on Ocean, Offshore and Arctic Engineering (OMAE2013). Nantes, France. https://doi.org/10.1115/OMAE2013-11425.

Vermeulen, H.R., 1995. Theory and practice of installing pipelines by the pre-snaking method. Proceedings of the 5th International Offshore and Polar Engineering Conference. The Hague, The Netherlands.

Wang, Z., Van Der Heijden, G.H.M., 2017. Localised lateral buckling of partially embedded subsea pipelines with nonlinear soil resistance. Thin-Walled Struct. 120, 408–420. https://doi.org/10.1016/j.tws.2017.05.017.

White, D.J., Westgate, Z., Ballard, J.-C., de Brier, C., Bransby, M.F., 2015. Best practice geotechnical characterization and pipe-soil interaction analysis for HPHT flowline design. Proc. Offshore Technology Conference. Houston. OTC26026-MS. https://doi.org/10.4043/26026-MS.